land

MDPI

Article

A Multi Source Data-Based Method for Assessing Carbon Sequestration of Urban Parks from a Spatial–Temporal Perspective: A Case Study of Shanghai Century Park

Yiqi Wang [1], Jiao Yu [1], Weixuan Wei [1,2] and Nannan Dong [1,*]

[1] College of Architecture and Urban Planning, Tongji University, Shanghai 200092, China; 2130146@tongji.edu.cn (Y.W.); 2310354@tongji.edu.cn (J.Y.); weiweixuan@tongji.edu.cn (W.W.)
[2] Future Urban (Shanghai) Design Consulting Co., Ltd., Shanghai 200092, China
* Correspondence: dongnannan@tongji.edu.cn

Abstract: As urbanization accelerates globally, urban areas have become major sources of greenhouse gas emissions. In this context, urban parks are crucial as significant components of carbon sinks. Using Shanghai Century Park as a case study, this study aims to develop an applicable and reliable workflow to accurately assess the carbon sequestration capacity of urban parks from a spatial–temporal perspective. Firstly, the random forest model is employed for biotope classification and mapping in the park based on multi-source data, including raw spectral bands, vegetation indices, and texture features. Subsequently, the Net Primary Productivity and biomass of different biotope types are calculated, enabling dynamic monitoring of the park's carbon sequestration capacity from 2018 to 2023. Moreover, the study explores the main factors influencing changes in carbon sequestration capacity from the management perspective. The findings reveal: (1) The application of multi-source imagery data enhances the accuracy of biotope mapping, with winter imagery proving more precise in classification. (2) From 2018 to 2023, Century Park's carbon sequestration capacity showed a fluctuating upward trend, with significant variations in the carbon sequestration abilities of different biotope types within the park. (3) Renovation and construction work related to biotope types significantly impacted the park's carbon sequestration capacity. Finally, the study proposes optimization strategies focused on species selection and layout, planting density, and park management.

Keywords: carbon sequestration; biotope mapping; spatial–temporal change; urban park

check for updates

Citation: Wang, Y.; Yu, J.; Wei, W.; Dong, N. A Multi Source Data-Based Method for Assessing Carbon Sequestration of Urban Parks from a Spatial–Temporal Perspective: A Case Study of Shanghai Century Park. *Land* **2024**, *13*, 1914. https://doi.org/10.3390/land13111914

Academic Editor: Marko Scholze

Received: 17 October 2024
Revised: 8 November 2024
Accepted: 13 November 2024
Published: 14 November 2024

Copyright: © 2024 by the authors. Licensee MDPI, Basel, Switzerland. This article is an open access article distributed under the terms and conditions of the Creative Commons Attribution (CC BY) license (https://creativecommons.org/licenses/by/4.0/).

1. Introduction

Cities, which are home to more than half of the world's population, account for approximately 70% of global greenhouse gas emissions, making them central to addressing climate challenges [1]. Enhancing carbon sequestration and reducing carbon emissions in urban areas have been recognized as two vital ways to achieve climate change mitigation and adaptation.

The United Nations' 2030 Agenda for Sustainable Development underscores the strategic importance of urban green spaces. As key representatives, urban parks deliver significant ecosystem services, including carbon sequestration (CS), urban cooling, air purification, etc. [2]. From a life cycle assessment perspective, urban parks generally function as net carbon sinks [3]. The vegetation in urban parks can effectively sequester carbon dioxide (CO_2) through photosynthesis, leading to a reduction in atmospheric CO_2 within urban environments [4]. Shadman et al. conducted a study on a 0.7-hectare urban park, calculating its CS potential over its entire life cycle. The findings indicated that the park has a substantial carbon sequestration capacity, amounting to 660.8 tCO_2e [5]. Similarly, Singkran estimated the total CS for 25 parks in Bangkok, covering a total area of 6.29 km^2. The results showed a total sequestration of 49,279 tCO_2e for the year 2020, representing approximately 0.1% of the city's total greenhouse gas emissions [6]. Given

the critical role of parks in urban carbon balance, there has been a growing focus among researchers and policymakers in recent years on quantitatively assessing and monitoring urban parks' CS capacity.

The CS capacity of vegetation can be represented and estimated through two indicators, net primary production (NPP) and biomass [7]. NPP is the total organic matter produced by plants through photosynthesis [8,9] and is commonly recognized as a key variable for assessing CS capacity [10,11]. Kil et al. selected NPP as a key indicator to evaluate the CS capacity of different biotope types in Seoul. The results indicated that forest areas had the highest NPP value, averaging 250.188 $gC \cdot m^{-2} \cdot a^{-1}$ [12]. Biomass is another important indicator that can indicate the total mass of organic material assembled by photosynthesis of vegetation [13]. Dash et al. conducted field surveys and recorded trees meeting the diameter at breast height criteria in ten urban parks in India to estimate park biomass and biomass carbon storage, concluding that the average biomass per hectare in parks was estimated to be 32.85 tC [14]. Kim et al. combined modeling with a field survey to assess the CS of specific tree species in urban parks, concluding that the average carbon storage in a 5.74 ha urban park was 15.30 $tC \cdot ha^{-1}$ [15].

CS estimation methods based on field survey data allow for precise assessment in small-scale areas. Based on the field survey of individual plant CS, Wang et al. mapped the spatial distribution of CS efficiency across 28 urban parks in Beijing [16]. Zhao et al. conducted empirical measurements of the CS capacity of plant communities with varying structural characteristics and discussed the influencing factors [17]. These studies required extensive field survey data, demonstrating an advantage in the reliability and accuracy of the estimation. Developed by the US Department of Agriculture, the i-Tree model is broadly used to estimate the CS of individual trees, which relies on accurate measurements of tree attributes comprising tree species, dimension, condition, etc. [15,18]. However, this method has several limitations. It is both time-consuming and labor-intensive and cannot assess CS for past years. Furthermore, applying vegetation data to regions with different geographical and climatic conditions may result in inaccurate estimations [19].

To directly estimate the CS capacity of an entire region, modeling and algorithmic computations based on remote sensing images are widely employed due to its effectiveness and efficiency. Xu et al. developed an optimized NPP estimation model based on the CASA model and adopted it for park green spaces in five cities. The result showed that the average NPP value of park green spaces in Shanghai was 686 $gC \cdot m^{-2} \cdot a^{-1}$ [20]. Similarly, Li et al. used an improved CASA model to quantify the CS efficiency of urban riverfront green spaces [21]. When applied to urban parks, this method often lacks sufficient detail in the division of CS estimation units and does not account for the specific characteristics of the park's vegetation. Consequently, this may result in inaccuracies in the estimation results.

With the improvement of sensor spatial resolution and advancements in remote sensing (RS) image processing technologies, RS-based CS estimation approaches have gained more attention in recent years [13,22]. A study from South Korea demonstrated the high potential of NIR and visible signatures to differentiate carbon sinks versus sources on a university campus. This offers insights into using spectral features of RS imagery for CS estimation of small-scale vegetation (the study area in this paper is 1.5 ha) [23]. Furthermore, in some studies, vegetation indices have been recommended and proven reliable for estimating the CS of plants, as they can accurately reflect the condition or growth of vegetation [19,24–26]. In the study of Wang et al., the CS efficiency of plant communities was based on the combined calculation of NPP, NDVI (Normalized Difference Vegetation Index), and LAI (Leaf Area Index) [16]. NDVI is widely used to assess vegetation, as it determines the amount and distribution of vegetation [27]. LAI, which measures the total single-side leaf area per unit of ground, is highly correlated with the aboveground carbon stock [28]. Additionally, texture features are used to characterize and differentiate surface properties in RS imagery, contributing to improved classification accuracy [26]. The study of Mngadi et al. quantified carbon stock variability across tree species by using texture

features derived from Sentinel-2 imagery via the gray level co-occurrence matrix (GLCM), followed by CS estimation using a machine learning algorithm [29].

Biotope mapping was first proposed by German scholars in the 1970s as part of a nature conservation strategy [30,31]. Compared to the land use and land cover (LULC) classification system commonly used in city-scale planning, biotope mapping offers a variable-scale classification of environmental units within a landscape, thereby playing a crucial role in delivering functional information about urban habitats [32–34]. Some researchers have applied biotope mapping for surface landscape classification in urban parks, enabling precise CS estimation, which then informed ecological management strategies and planning [16,17,35].

With the increasing recognition of urban parks as important carbon sinks, park management authorities are placing greater emphasis on strategies to enhance parks' capacity to offset carbon emissions [36,37]. Therefore, it is crucial to obtain the spatial patterns of CS in urban parks and dynamically monitor their CS capacity. This study addresses the following question: How can an applicable and reliable workflow be developed to accurately evaluate the CS capacity of urban parks from a spatial–temporal perspective? To achieve this, we first classified and mapped the biotopes in Century Park using a multi-source data-based method. Based on the biotope maps, we then assessed the CS capacity of Century Park over a six-year period. The changing characteristics of CS capacity and potential influencing factors were subsequently analyzed. Finally, we proposed planting and management strategies aimed at enhancing the CS capacity of urban parks, thereby contributing to the development of low-carbon, sustainable cities.

2. Materials and Methods

2.1. Study Area

Located in the eastern coastal region of China, Shanghai has a northern subtropical monsoon climate and experiences four distinct seasons. The annual average temperature in Shanghai is 17.9 °C. Summers are hot and humid, while winters are cold and dry. Approximately 81% of the annual precipitation occurs between April and October, with an average annual rainfall of 1388.2 mm (2021 data provided by the Shanghai Meteorological Bureau).

As a leading megacity in China, Shanghai's carbon emissions are notably high [38]. Shanghai also ranks high in carbon emissions. It is projected that Shanghai's annual CO_2 emissions will peak in 2024 at approximately 200 million tons [39]. Enhancing the carbon sequestration capacity of urban parks is a key focus for Shanghai in achieving its 2030 carbon peaking and carbon neutrality goals [40].

This study was conducted in the 147.2 ha Shanghai Century Park (Figure 1), characterized by its prolonged history and diverse vegetation types. Lying in the central urban area, it is one of the largest parks in Shanghai, which holds significant importance to the carbon balance of both Pudong District and the entire city. Century Park was built in 1995 and has been open to public since 2000. There are seven landscape zones in the park divided by the features and characteristics, including the Lakeside Scenic Zone (33.6 ha), Scenic Forest Zone (19.8 ha), Open Woodland and Grassland Zone (20.7 ha), Bird Protection Zone (12.6 ha), Native Countryside Zone (24.5 ha), Exotic Garden Zone (23.4 ha), and Golf Course Zone (12.6 ha).

2.2. Methodological Framework

The primary objective of this study was to develop an applicable and practical workflow for assessing the CS capacity of urban parks and its spatial–temporal variations (Figure 2). First, we applied an optimized random forest (RF) model to classify biotope types in Century Park using Sentinel-2 imagery. Second, we used the CS model from the IMECOGIP Toolbox to calculate the park's NPP and biomass. We then analyzed changes in NPP and biomass across the entire park from 2018 to 2023. Three landscape zones were selected to examine factors influencing CS capacity. Finally, we provided management and development recommendations based on these findings.

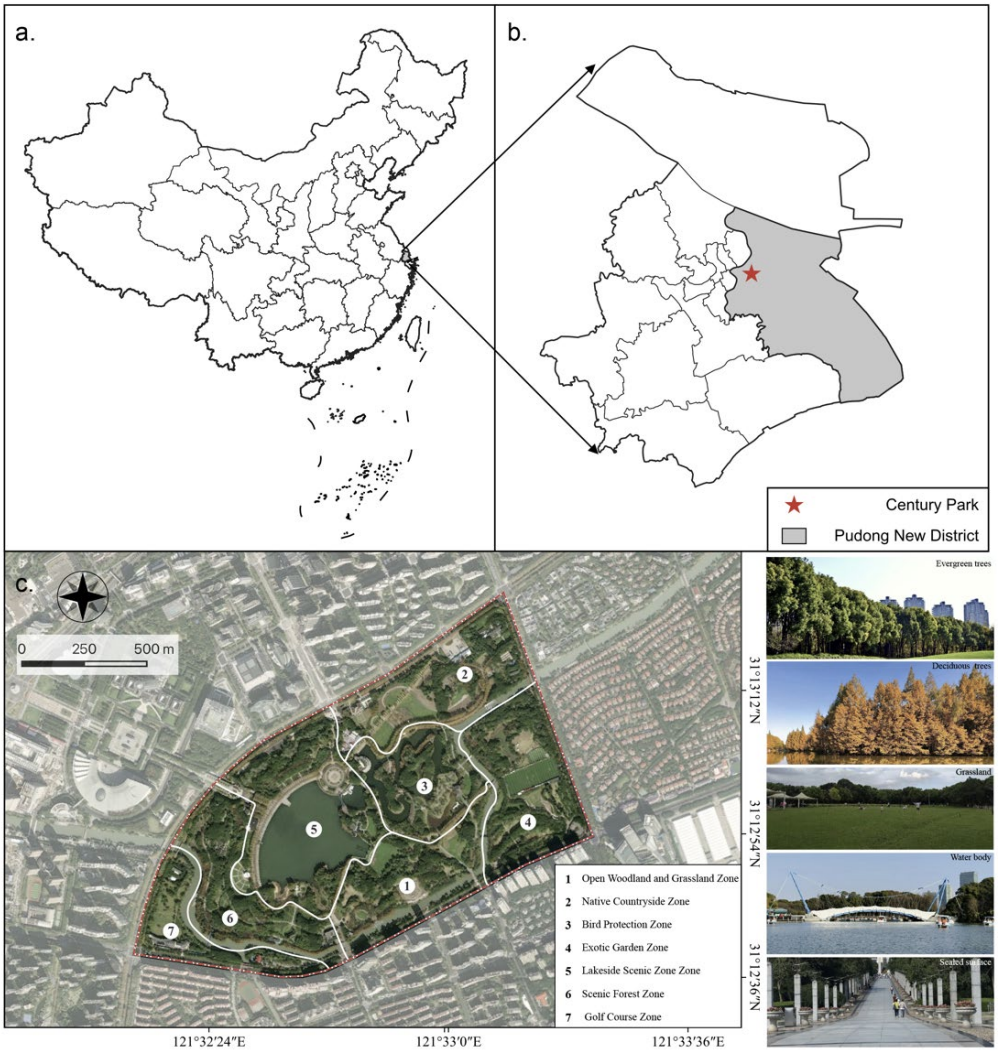


Figure 1. Location of the study area: (**a**) China; (**b**) Pudong New District, Shanghai; (**c**) Century Park.

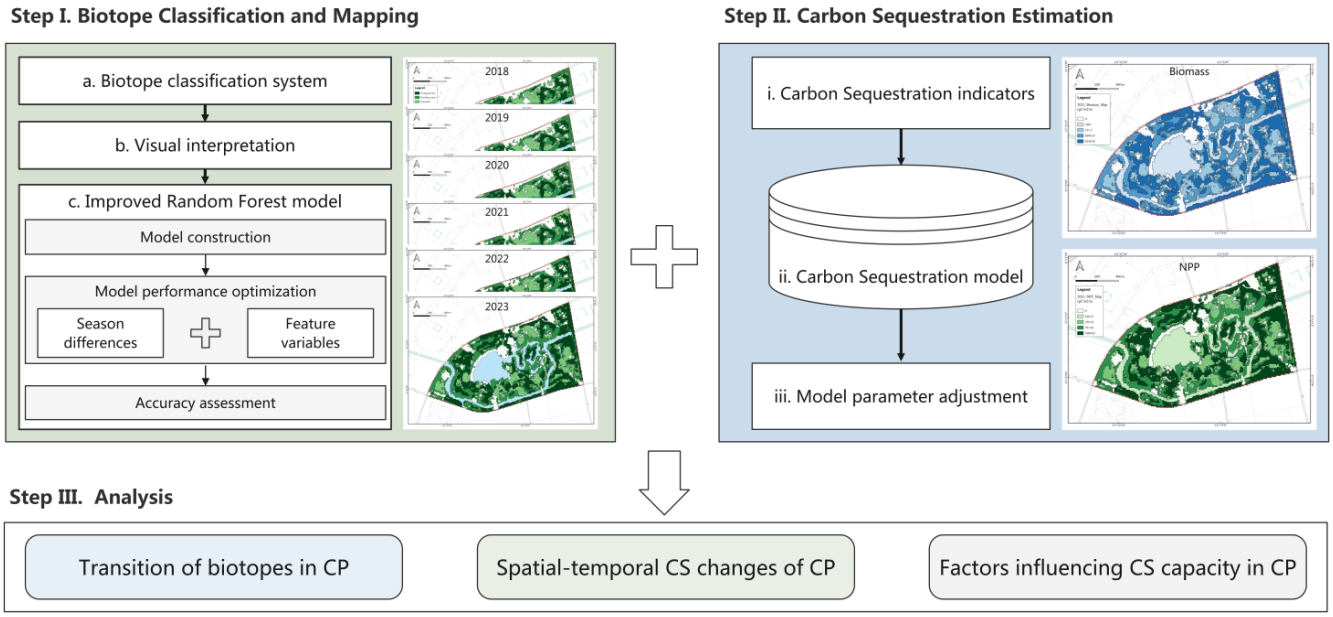


Figure 2. Flowchart of methodology.

2.3. Biotope Classification and Mapping

2.3.1. Biotope Classification System of Urban Parks

In Jia et al.'s previous study, the land cover of the China Green Expo Park was categorized into 4 types (high vegetation, low vegetation, sealed surfaces, and water body), which, however, neglected the variance of CS capacity between evergreen trees and deciduous trees [41].

Based on existing biotope classification systems, we developed a refined hierarchical classification structure tailored to Century Park's unique characteristics. This system categorizes biotopes into three primary levels: green, blue, and gray spaces. Within the first level, green space is defined by areas dominated by vegetation, blue space by water bodies, and gray space by artificial surfaces. The second level further differentiates these spaces by specifying the primary vegetation or material present, such as evergreen or deciduous trees in green spaces and water bodies in blue spaces. The third level provides detailed descriptions of the specific types of vegetation or surfaces found within each category, including grasslands, shrubs, and sealed surfaces. Table 1 summarizes these classifications, aligning with the descriptions provided.

Table 1. Biotope classification system of Century Park.

Level 1: Land Cover	Level 2: Biotope Type	Description	Code
Green Space	Evergreen tree	Forest dominated by evergreen tree species	AA
	Deciduous tree	Forest dominated by deciduous tree species	AB
	Meadow/small woods	Composed of single herbaceous plants or scattered shrubs	GD
Blue Space	Water body	Area covered by water surfaces, including lakes, ponds, rivers, etc.	F
Gray Space	Sealed surface	Area covered by artificial hard materials, including buildings, roads, parking lots, and paved surfaces	NF

2.3.2. Visual Interpretation for Biotope Classification

The sample size for RF classification is mainly determined by the area and the quantity of land cover types. In general, at least 50 sample points should be selected per biotope type [39]. In this study, we constructed a dataset of 602 sample points by visually interpreting and categorizing the five main biotope types in Century Park. This dataset includes 120 points for evergreen tree forests, 122 points for deciduous tree forests, 124 points for meadows, 113 points for water bodies, and 123 points for sealed surfaces.

2.3.3. Improved Random Forest Model for Biotope Classification

1. Construction of RF model

Due to our inability to obtain historical biotope information of Century Park through field surveys, this study explores methods to identify and map biotopes based on remote sensing imagery using supervised pixel-based classification algorithms. Common algorithms include Maximum Likelihood Classification, Support Vector Machine, Decision Tree, and Random Forest. Among these, the Random Forest model has been proven in other studies to exhibit a better performance in classification, attracting significant attention in recent years.

RF constructs multiple decision trees during the model training phase. Each tree is built based on bootstrapped samples of the original dataset and random feature selection. Compared to a single decision tree, RF accounts for the variability among individual trees, thereby reducing the risk of overfitting and enhancing the overall predictive performance of the model. For classification tasks, RF aggregates the results of all decision trees through voting, producing stable and accurate predictions. Consequently, RF is widely applied in spatial land use classification studies. The schematic diagram of RF for classification is illustrated in Figure 3.

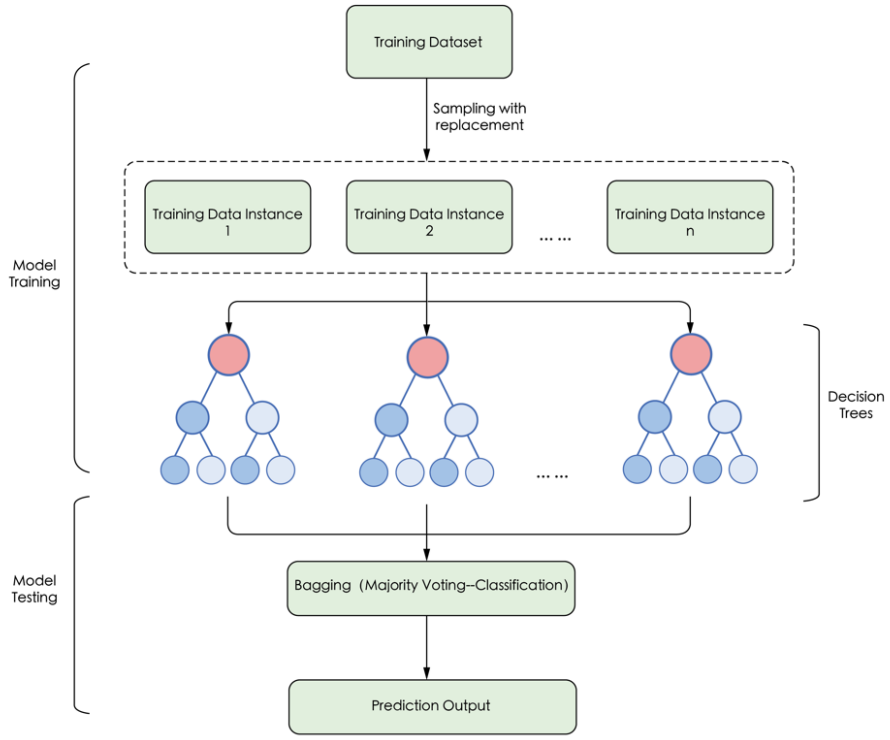


Figure 3. Schematic diagram of Random Forest model for image classification.

In this study, we constructed an RF model to classify and map the biotope types in Century Park. The dataset consists of 612 randomly distributed ground truth points, which are divided into a training set and a test set in an 8:2 ratio. The number of decision trees was set to 50.

2. Variables improving model performance

The performance of an RF model can be influenced by various variables, including targeted classes and other uncertain variables [42]. In order to enhance the model's accuracy, we explored and compared the classification results utilizing different imagery data accessed from the summer and winter periods, as well as the feature variables involved.

(1) Classification difference between the two time periods

Evergreen trees retain green foliage throughout the year, while deciduous trees display pronounced seasonal changes, with green leaves in summer that shed in winter. Based on this, we could distinguish between the two biotope types in Century Park according to their differences in many spectral features.

(2) Classification difference contributed by multiple feature variables

a. Sentinel-2, Level-2A delivers information in 13 spectral bands, including visible (Blue, Green, Red), near-infrared (NIR), and shortwave infrared (SWIR) bands, etc. Each band has distinct properties and reveals specific spectral features of various objects in the image.

b. Vegetation indices, which can convey important information on the condition of the and cover, are of great importance to vegetation extraction and classification, and are widely used in relevant studies [43,44]. In this study, the selection of vegetation indices was informed by prior research and tailored to the park's distinctive features. Given that Century Park is mainly covered by vegetation (approximately 68%) and water (approximately 20%), during the study period, NDVI, LAI, FVC (Fractional Vegetation Cover), and EVI (Enhanced Vegetation Index) were considered as key indices when it came to mapping the biotopes. The formulas are summarized in Table 2.

Table 2. Vegetation indices used for vegetation and classification.

Index	Equation	Definition	No.
NDVI	$NDVI = \frac{(NIR-RED)}{(NIR+RED)}$	To evaluate the vegetation condition and growth status in the park, with a range of [−1, 1].	(1)
LAI	$LAI = a \times EVI - b$	To describe the ratio of the projected area of vegetation leaves in the vertical direction to the unit area of the park, with a range of [0, ∞].	(2)
FVC	$FVC = \frac{NDVI-NDVI_{soil}}{NDVI_{veg}-NDVI_{soil}}$	To describe the proportion of the park covered by vegetation, with a range of [0, 1].	(3)
EVI	$EVI = G \times \frac{NIR-RED}{NIR+C1\times RED-C2\times BLUE+L}$	To assess the vegetation growth status and ecological environment quality in the park, with a range of [−1, 1].	(4)

c. Besides the feature variables mentioned above, texture features play a crucial supportive role in enhancing the accuracy of remote sensing image classification according to existing studies. The Gray-Level Co-occurrence Matrix (GLCM), which was proposed by Haralick in 1973, has been proven to be one of the most widely used methods for extracting texture features from images. We selected and computed four texture features from the GLCM, i.e., GLCM sum average, GLCM contrast, GLCM sum variance, and GLCM difference variance. The formulas are as follows:

$$SumAva = \sum_{i=2}^{2N_g} ip_{x+y}(i) \quad (5)$$

$$Con = \sum_{n=0}^{N_g-1} n^2 \left\{ \sum_{i=1}^{N_g} \sum_{j=1}^{N_g} p(i,\ j) \right\},\ |i-j| = n \quad (6)$$

$$SumVar = \sum_{i=2}^{2N_g} (i-f_s)^2 p_{x+y}(i) \quad (7)$$

$$DifVar = \sum_{i=0}^{N_g-1} i^2 p_{x-y}(i) \quad (8)$$

in which x and y are the coordinates (row and column) of an entry in the co-occurrence matrix, and $p_{x+y}(i)/p_{x-y}(i)$ is the probability of the co-occurrence matrix coordinates summing to $x+y/x-y$.

In this study, we established four distinct variable groups for comparison: summer and winter imagery utilizing only spectral bands and summer and winter imagery incorporating multiple feature variables. RF models were constructed for each group to classify the biotopes in Century Park.

3. Accuracy assessment of the classification results

To test the performance of each RF model, accuracy assessment was conducted based on the Confusion Matrix, introduced by Karl Pearson in 1904. The Confusion Matrix provides various performance metrics, among which overall accuracy (OA) and Kappa coefficient were selected in this study.

The overall accuracy (OA) is a metric used to evaluate the classification accuracy of the RF model. It is defined as the ratio of the number of correctly classified samples to the total number of samples, calculated as shown in Equation (1). Additionally, the Kappa coefficient is commonly used to assess classification accuracy. The Kappa coefficient ranges from −1 to 1, with higher values indicating greater agreement between observed and predicted values. Specifically, a Kappa coefficient between 0.41 and 0.60 indicates moderate agreement, between 0.61 and 0.80 indicates substantial agreement, and values above 0.80 indicate almost perfect agreement. The formula for calculating the Kappa coefficient is presented in Equation (2).

$$OA = \frac{T}{N} \quad (9)$$

$$Kappa = \frac{P_o - P_e}{1 - P_e} \quad (10)$$

$$P_e = \sum\left(\frac{r_i * c_i}{N^2}\right) \quad (11)$$

in which T is the number of correctly classified samples and N is the total number of samples in Equation (9). P_o represents the observed accuracy, which is the overall accuracy calculated by Equation (9), while P_e denotes the expected accuracy from random classification in Equation (10). For Equation (11), r_i is the proportion of true samples of class, i in the total sample, and c_i is the proportion of predicted samples of class i in the total sample.

2.4. CS Estimation

2.4.1. CS Indicators

NPP and biomass are widely used indicators for assessing the CS potential of vegetation. NPP represents the annual carbon remaining after respiration losses, while biomass reflects the accumulated NPP minus litterfall, representing the standing mass of the vegetation [45,46].

2.4.2. CS Estimation Model

In this study, we calculated the CS capacity of the entire park based on the CS capacity per unit area of different biotope types and the corresponding areas of each biotope, as shown in Equation (12). For this calculation, we employed the EnhancES toolbox on QIS 3.34.7-Prizren, developed by the Institute of Geography at Ruhr University Bochum [47].

$$C_{tot} = \sum_{i=1}^{n} C_i \times S_i \quad (12)$$

in which C_{tot} is the annual total carbon sequestration of the park ($gC \cdot a^{-1}$); C_i is biotope i's annual carbon sequestration (NPP and biomass) density ($gC \cdot m^{-2} \cdot a^{-1}$); and S_i is biotope i's area (m^2).

2.4.3. Model Parameter Adjustment

Due to the regional differences in vegetation carbon sequestration capacity, it would be inappropriate to directly adopt the default NPP and biomass densities offered in the toolbox. Thus, referring to the literature [48,49], the annual carbon sequestration densities of the following five biotope types in Century Park were estimated (Table 3). The formula used is given in Equation (13).

$$C_i = \sum_{j=1}^{n} D_j \times R_j \quad (13)$$

in which C_i is biotope i's annual NPP/biomass density ($gC \cdot m^{-2} \cdot a^{-1}$); D_j is vegetation type j's average NPP/biomass density ($gC \cdot m^{-2} \cdot a^{-1}$); and R_j is vegetation type j's area proportion in biotope i.

Table 3. Calculation of average NPP and average biomass density.

Biotope Types	Vegetation Types	Proportion (%)	Biomass Density ($gC \cdot m^{-2} \cdot a^{-1}$)	Average Biomass Density ($gC \cdot m^{-2} \cdot a^{-1}$)	NPP Density ($gC \cdot m^{-2} \cdot a^{-1}$)	Average NPP Density ($gC \cdot m^{-2} \cdot a^{-1}$)
Evergreen Trees	Camphor Tree	38.30	5680	5234.09	751	688.12
	Cedar	4.85	830		690	
	Privet	56.85	5310		170.4	
Deciduous Trees	Dawn Redwood	45.34	2980	2813.94	690	524.64
	Poplar	22.99	3265		719.5	
	Willow	11.58	1785		507	
	Plane Tree	11.48	1988		537.5	
	Ginkgo	8.61	3220		89.9	

Table 3. *Cont.*

Biotope Types	Vegetation Types	Proportion (%)	Biomass Density ($gC \cdot m^{-2} \cdot a^{-1}$)	Average Biomass Density ($gC \cdot m^{-2} \cdot a^{-1}$)	NPP Density ($gC \cdot m^{-2} \cdot a^{-1}$)	Average NPP Density ($gC \cdot m^{-2} \cdot a^{-1}$)
	Grassland			131.5		259.18
	Water Body			1081		108.12
	Sealed surface			0		0

2.5. Data Collection and Preprocessing

2.5.1. Satellite Image Processing

Google Earth Engine (GEE) (https://earthengine.google.com/, accessed on 4 February 2024) is a cloud-based platform for planetary-scale environmental data collection, analysis, and visualization which provides much convenience in the acquisition and processing of remote sensing images. In this regard, we accessed the "Harmonized Sentinel-2 MSI: MultiSpectral Instrument, Level-2A" imagery dataset and then carried out our pre-processing work on GEE. It is worth noting that this dataset offers surface reflectance data with a spatial resolution of 10 m from March 2017 to July 2024 (accessed on 25 July 2024) that has undergone geometric calibration and atmospheric correction, thus simplifying the data pre-processing workflow. Then, we retrieved and filtered Sentinel-2 Level-2A data covering the study area with less than 10% cloudiness. Meanwhile, taking into account the meteorological conditions in Shanghai, we designated July and August as the summer period and December and January (the next year) as the winter period in this study. Considering the availability of the images, Sentinel-2A imagery data in both summer and winter periods between 2018 and 2023 were captured, respectively. Finally, we selected the median image for each period each year from the image collection as the representative for subsequent study.

2.5.2. CS Capacity of Different Tree Species

In this study, we consulted the relevant literature and experimental data to determine the CS capacity of various tree species. We also obtained data from the existing literature on the types and quantities of major tree species in Century Park in 2009 [50].

2.5.3. Urban Park Construction and Renovation Data

To determine the reasons for the dynamics of carbon sequestration of Century Park, we conducted face-to-face interviews with designers who were in charge of the renovation work, as well as staff from the management office of the park. Through the interview, spatial data on park construction and renovation from 2018 to 2020 were collected.

3. Results

3.1. RF Model Classification Results

By testing the four RF classification models mentioned in Section 2.4.2 and conducting accuracy assessments using the confusion matrix, respectively, we obtained the classification accuracy results shown in Figure 4.

By comparing and analyzing the results shown in the figures, it is evident that the RF classifier developed in this study demonstrates higher accuracy in identifying biotope types and overall classification precision for winter imagery compared to summer imagery, regardless of whether it is based on raw spectral band data or multi-source feature data. Regarding the Kappa coefficient, an indicator for evaluating the performance of RF models, the results also show higher accuracy and consistency for winter imagery.

Taking 2023 as an example, the OA of the RF classification based on summer Sentinel-2 imagery was 0.783 (raw spectral bands) and 0.8167 (multi-source data), while the overall accuracy for winter imagery was 0.8580 (raw spectral bands) and 0.8583 (multi-source data), representing increases of 9.58% (raw spectral bands) and 5.09% (multi-source data), respectively. The Kappa coefficients for the winter imagery-based RF classifiers were 0.8280

(raw spectral bands) and 0.8226 (multi-source data), reflecting improvements of 13.58% and 6.75% compared to the summer imagery-based classifiers.

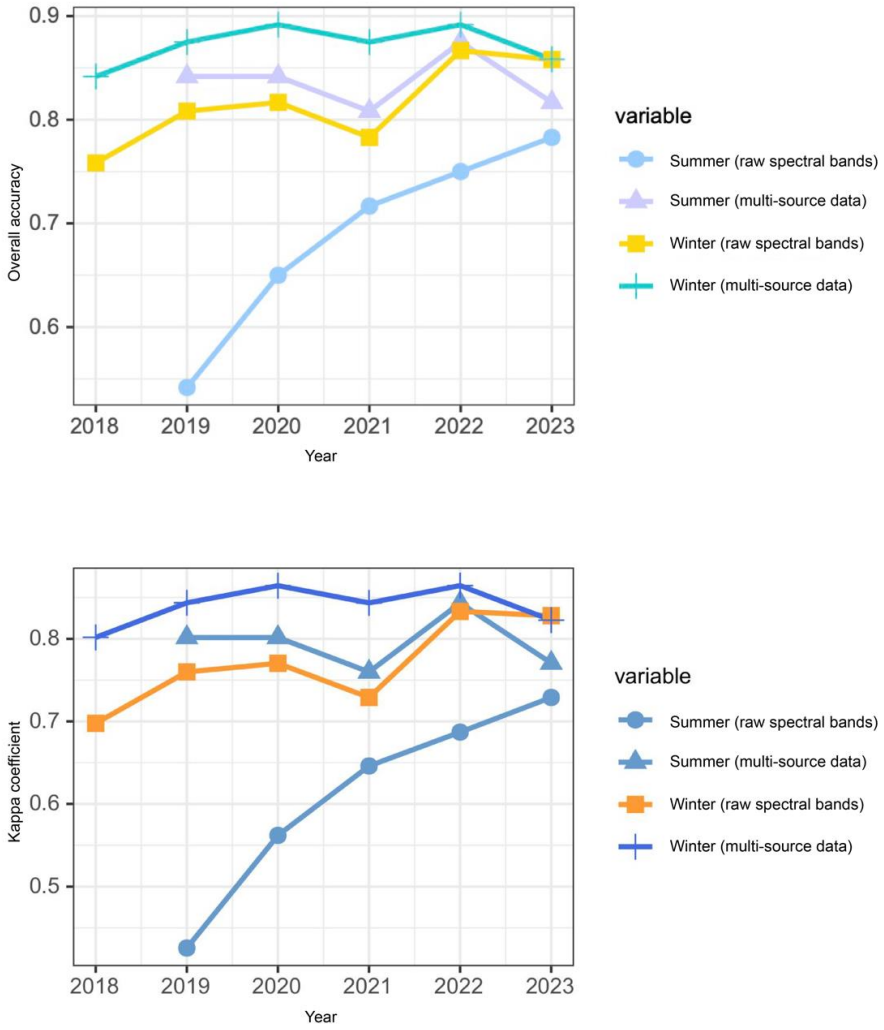


Figure 4. Accuracy assessment of classification results from four RF models ((**top**): overall accuracy; (**bottom**): Kappa coefficient).

Another comparison reveals that incorporating vegetation indices into the input base imagery significantly impacts the RF classification accuracy. When four vegetation indices were added to the raw spectral band information as input attributes for classification training and validation, the classification accuracy improved. For instance, in 2019, the RF classifier based on multi-source data achieved 55.38% (summer) and 8.25% (winter) increases in overall accuracy compared to the classifier based only on raw spectral band information. Correspondingly, the Kappa coefficient improved by 88.35% (summer) and 11.01% (winter).

In conclusion, to select the most accurate and representative classification results for mapping the biotope types of Century Park during the study period, we ultimately used winter Sentinel-2 imagery as the original data source. We combined raw spectral bands with vegetation indices as multi-source input data for RF classification, resulting in six annual biotope type maps of Century Park from 2018 to 2023 (Appendix A).

3.2. Changes in Biotopes of Century Park

The study selected the years 2018, 2020, and 2023 as representative years, gathering data on the area of biotope types within Century Park for each of these years. Transition matrices for the periods 2018–2020 and 2020–2023 were constructed, as shown in Table 4,

Figure 5, Table 5, and Figure 6, respectively, to analyze the transitions between different biotope types within the park. These matrices provide a basis for understanding the spatial and temporal evolution of carbon sequestration capabilities in Century Park, offering insights into the underlying reasons for the observed changes.

Table 4. Transition matrix of biotope types in Century Park from 2018 to 2020.

	Evergreen Trees	Deciduous Tree	Grassland	Water Body	Sealed Surface	2018	Outflow Area
Evergreen Trees	30.524	5.894	1.429	0.163	0.290	38.300	7.776
Deciduous Tree	4.602	31.200	6.072	1.422	2.132	45.428	14.228
Grassland	1.338	1.927	16.752	0.068	2.208	22.294	5.541
Water Body	0.164	1.885	0.119	23.890	0.418	26.476	2.586
Sealed Surface	0.848	3.018	2.700	0.303	14.823	21.693	6.870
2020	37.477	43.923	27.073	25.846	19.871	/	/
Inflow Area	6.952	12.723	10.321	1.957	5.048	/	37.001

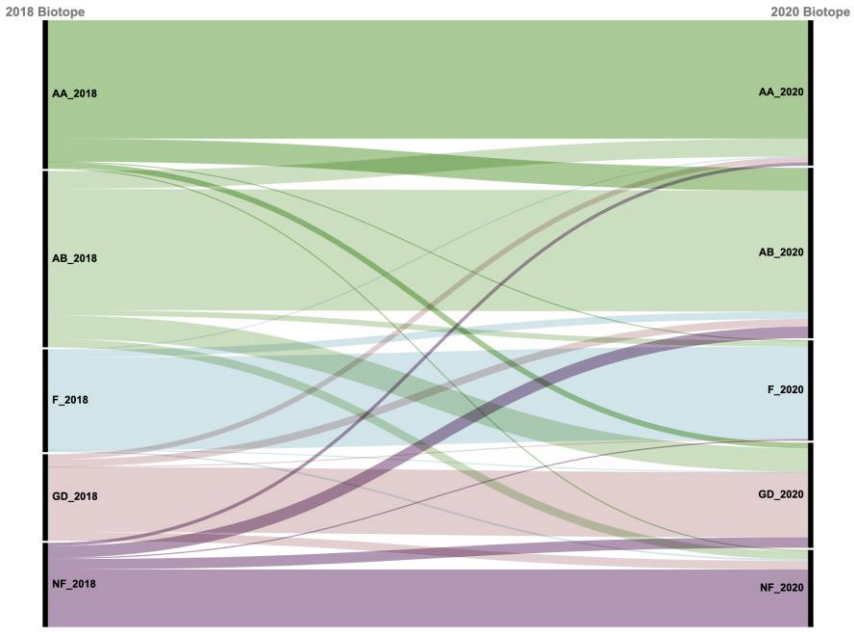


Figure 5. Schematic diagram of biotope type transitions in Century Park from 2018 to 2020.

Table 5. Transition matrix of biotope types in Century Park from 2020 to 2023.

	Evergreen Trees	Deciduous Tree	Grassland	Water Body	Sealed Surface	2020	Outflow Area
Evergreen Trees	29.747	3.443	3.752	0.095	0.439	37.477	7.729
Deciduous Tree	11.196	25.326	3.864	1.375	2.162	43.923	18.597
Grassland	3.993	4.015	15.755	0.085	3.225	27.073	11.318
Water Body	0.439	0.933	0.140	23.516	0.818	25.846	2.330
Sealed Surface	1.247	2.668	2.457	0.554	12.944	19.871	6.926
2023	46.622	36.386	25.969	25.625	19.588	/	/
Inflow Area	16.875	11.060	10.214	2.109	6.644	/	46.902

Table 4 displays the transition matrix for biotope types within Century Park from 2018 to 2020. During this period, the total area of biotope types that experienced change was 37.00 hm^2, accounting for 24% of the park's total area. The most significant transitions occurred among grasslands, deciduous trees, and evergreen trees. Deciduous trees had the largest area of transition, with 14.23 hm^2 transitioning out, accounting for 38.45% of the total transition out. Evergreen trees followed, with 7.78 hm^2 transitioning out, representing 21.02% of the total. In terms of areas transitioning in, deciduous trees again led with 12.72 hm^2, followed by grasslands with 10.32 hm^2, comprising 34.39% and 27.90% of the total transition in, respectively.

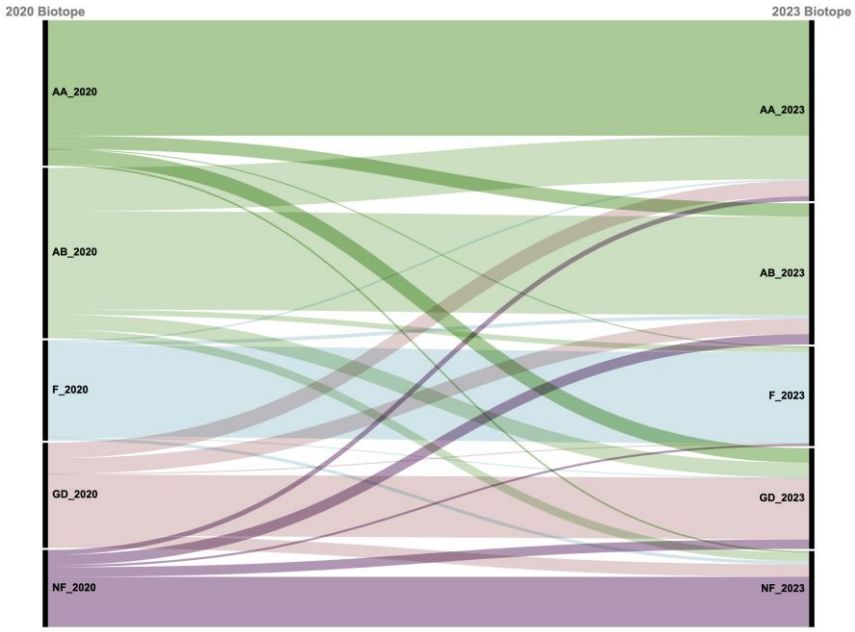


Figure 6. Schematic diagram of biotope type transitions in Century Park from 2020 to 2023.

A detailed analysis reveals that a significant portion of deciduous trees transitioned into grasslands (6.07 hm^2) and evergreen forests (4.60 hm^2), accounting for 13.37% and 10.13% of the deciduous tree area in 2018, respectively. Simultaneously, some evergreen trees transitioned into deciduous trees, amounting to 15.39% of the evergreen forest area in 2018. Overall, the total area changes between 2018 and 2020 were relatively small, with an increase in grasslands (4.78 hm^2) and deciduous trees (1.50 hm^2) and a decrease in sealed surfaces (1.82 hm^2). Other biotope types showed minimal area changes.

Table 5 presents the transition matrix for the period of 2020–2023. During this time, the total area of biotope type changes increased to 46.90 hm^2, representing 30.42% of the park's total area. Most transitions occurred among deciduous trees, grasslands, and evergreen trees. Deciduous trees had the largest area transitioning out (18.60 hm^2), accounting for 38.45% of the total transition out, followed by grasslands with 11.32 hm^2, representing 24.13%. In terms of areas transitioning in, evergreen trees saw the most significant increase, with 16.88 hm^2 transitioning in, accounting for 35.98% of the total, followed by deciduous trees (11.06 hm^2) and grasslands (10.21 hm^2), comprising 23.58% and 21.78% of the total transition in, respectively.

Specifically, deciduous trees mainly transitioned into evergreen trees, with 25.49% of the deciduous tree area in 2020 transitioning out. Overall, the total area of evergreen trees increased significantly (9.15 hm^2), mainly due to transitions from deciduous trees, resulting in a reduction in the total area of deciduous trees (7.54 hm^2). Other biotope types showed little change in area.

In summary, between 2018 and 2020 and from 2020 to 2023, the main transitions in area within Century Park occurred among evergreen trees, deciduous trees, and grasslands. Across the entire period, the area of evergreen trees increased the most, followed by grasslands, while the area of water bodies remained stable and the area of deciduous trees and sealed surfaces decreased. These changes suggest that certain areas of deciduous trees and sealed surfaces within Century Park may have been replaced or reforested with evergreen trees, leading to the observed area changes.

3.3. Temporal Changes in Total CS of Century Park

The spatial distribution of NPP and biomass values in Century Park is mapped based on the classification results. Figure 7 presents the NPP and biomass maps for 2023. From the perspective of changes in CS capacity, the trends in total biomass and NPP of Century Park

from 2018 to 2023 were consistent, both experiencing a process of initial decline followed by an increase, another decline, and a final rise. However, over a longer period, the CS capacity of Century Park shows an upward trend (Figure 8).

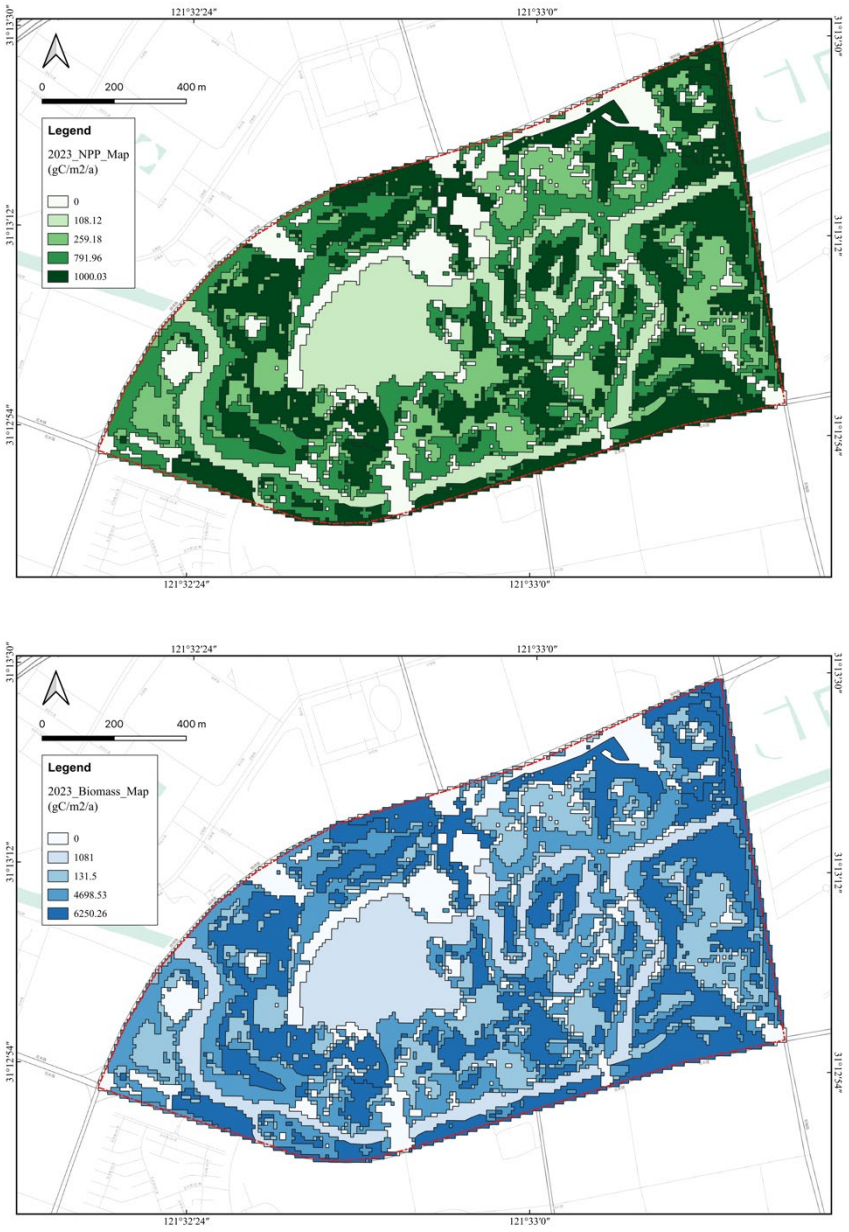


Figure 7. NPP (**top**) and biomass (**bottom**) map of Century Park in 2023.

From 2018 to 2020, the total biomass of Century Park decreased from 4746.57 tons of carbon to 4642.20 tons of carbon, a reduction of 104.37 tons of carbon over two years, representing a decline of 2.20%. Meanwhile, NPP decreased from 813.17 tons of carbon per year to 806.15 tons of carbon, a decline of 0.86%.

From 2020 to 2021, the total biomass increased from 4642.20 tons of carbon to 4690.87 tons of carbon, a total increase of 48.67 tons, representing a growth of 1.05%. NPP increased from 806.15 tons of carbon to 810.23 tons of carbon, an increase of 0.51%.

However, from 2021 to 2022, both biomass and NPP declined again, decreasing by 67.99 tons of carbon and 5.21 tons of carbon, respectively, representing decreases of 1.45% and 0.64%.

From 2022 to 2023, with the completion of vegetation renovation projects and the enhancement of maintenance measures and management, the total vegetation area and

growth condition in Century Park improved, leading to a significant increase in CS capacity. The total biomass increased from 4622.88 tons of carbon to 4797.55 tons of carbon, a total increase of 174.67 tons, representing a growth of 3.78%. NPP also increased from 805.02 tons of carbon to 827.04 tons of carbon, an increase of 22.02 tons, or 2.74%. The increases in both total biomass and NPP during 2022–2023 (3.78% and 2.74%, respectively) were significantly higher than those during 2020–2021 (1.05% and 0.51%, respectively).

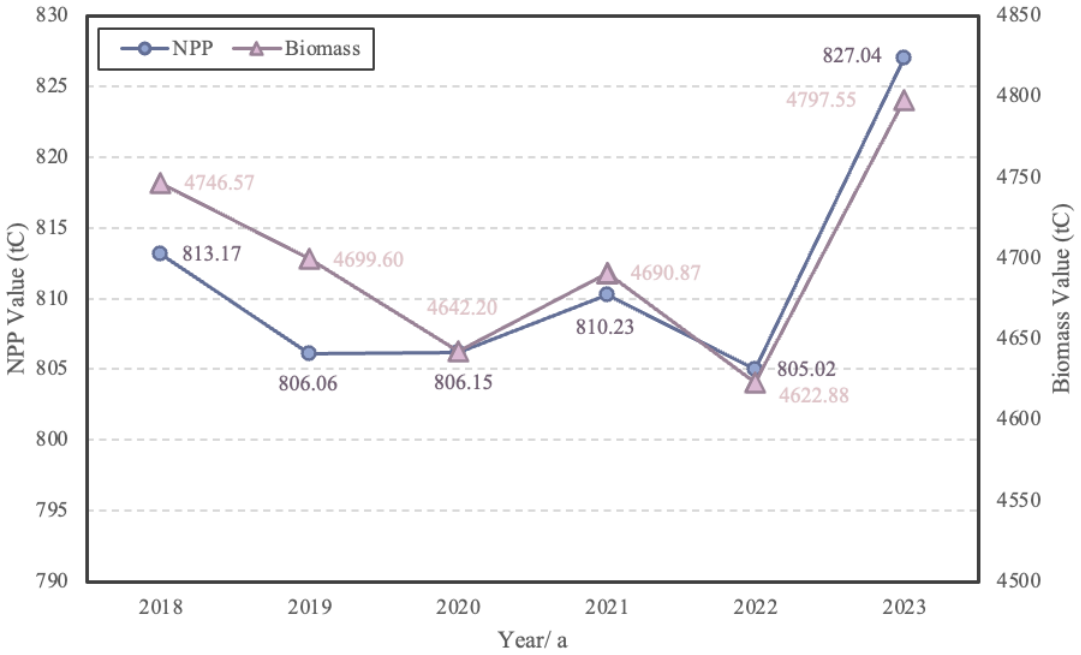


Figure 8. Variation in CS capacity of Century Park from 2018 to 2023.

3.4. Spatial Changes in CS Distribution of Century Park

3.4.1. Description of CS Changes of Different Zones

The biomass and NPP of each zone within Century Park were calculated annually, and the results are presented in Table 6, Table 7, Figure 9, and Figure 10, respectively.

Table 6. Annual biomass values for landscape zones in Century Park (tC).

Year	Open Woodland and Grassland Zone		Native Countryside Zone		Bird Protection Zone		Exotic Garden Zone		Lakeside Scenic Zone		Scenic Forest Zone		Golf Course Zone	
2018	703.04	14.81%	595.54	12.55%	561.51	11.83%	838.30	17.66%	821.60	17.31%	834.53	17.58%	392.05	8.26%
2019	685.05	14.58%	616.91	13.13%	507.32	10.80%	867.06	18.45%	788.62	16.78%	829.10	17.64%	405.53	8.63%
2020	662.17	13.46%	598.48	12.89%	511.57	11.02%	794.78	17.12%	849.35	18.30%	828.92	17.86%	396.93	8.55%
2021	631.42	13.46%	576.48	12.29%	533.51	11.37%	914.89	19.50%	808.21	17.23%	800.85	17.07%	425.51	9.07%
2022	666.76	14.42%	640.57	13.86%	492.90	10.66%	879.09	19.02%	781.46	16.90%	782.46	16.93%	379.64	8.21%
2023	626.26	13.05%	755.35	15.74%	511.17	10.65%	885.94	18.47%	855.67	17.84%	780.21	16.26%	382.95	7.98%

Table 7. Annual NPP values for landscape zones in Century Park (tC).

Year	Open Woodland and Grassland Zone		Native Countryside Zone		Bird Protection Zone		Exotic Garden Zone		Lakeside Scenic Zone		Scenic Forest Zone		Golf Course Zone	
2018	121.84	14.98%	113.79	13.99%	91.93	11.31%	148.91	18.31%	131.29	16.15%	137.38	16.89%	68.03	8.37%
2019	119.49	14.82%	116.24	14.42%	83.53	10.36%	153.29	19.02%	126.45	15.69%	137.24	17.03%	69.82	8.66%
2020	116.20	14.41%	117.31	14.55%	86.04	10.67%	143.78	17.84%	136.65	16.95%	137.46	17.05%	68.71	8.52%
2021	112.27	13.86%	111.80	13.80%	89.77	11.08%	159.76	19.72%	130.55	16.11%	133.21	16.44%	72.88	9.00%
2022	119.59	14.86%	120.43	14.96%	82.55	10.25%	156.18	19.40%	127.81	15.88%	132.27	16.43%	66.19	8.22%
2023	114.48	13.84%	134.75	16.29%	83.85	10.14%	156.23	18.89%	138.68	16.77%	131.94	15.95%	67.11	8.12%

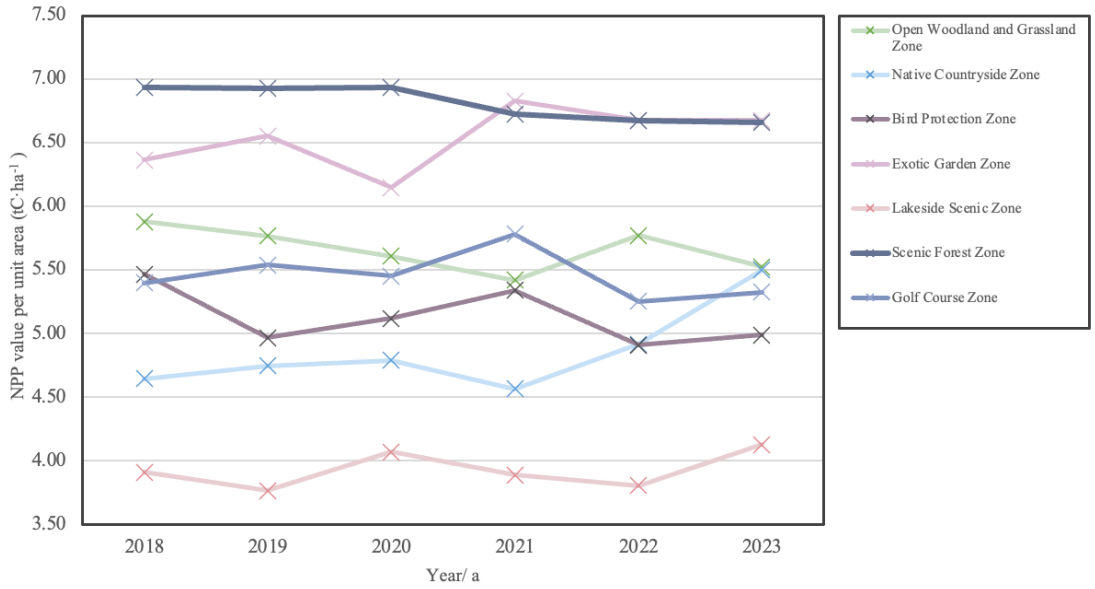


Figure 9. Variation in NPP per unit area for landscape zones in Century Park from 2018 to 2023.

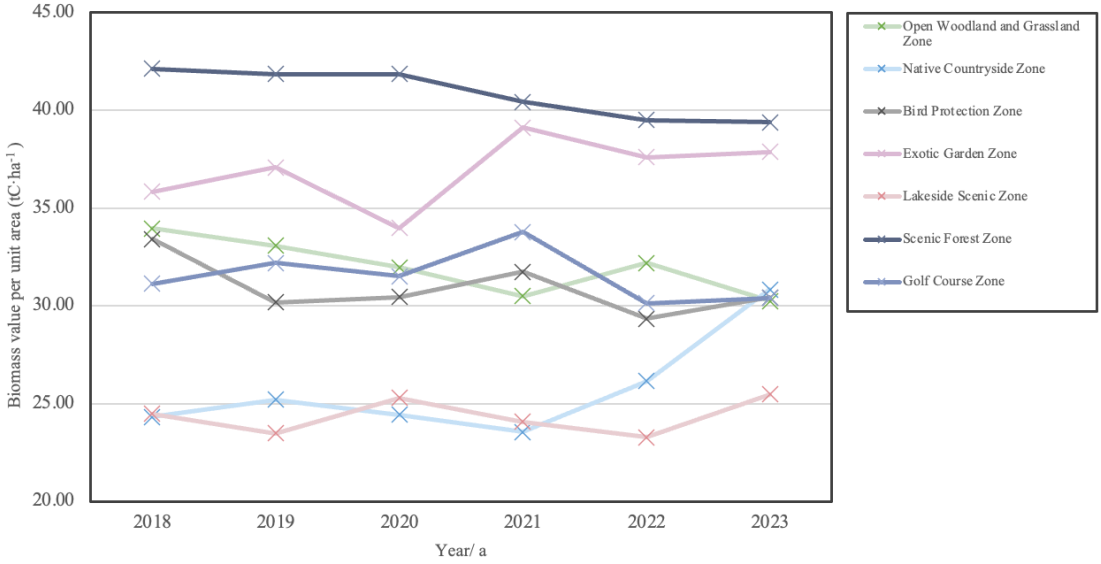


Figure 10. Variation in biomass per unit area for landscape zones in Century Park from 2018 to 2023.

From the data presented in Tables 6 and 7, it is evident that the Exotic Garden Zone contributes the most to the overall carbon sequestration of Century Park. This zone has consistently maintained its leading position, with its annual CS contribution exceeding 17.1% (biomass) and 17.8% (NPP). Additionally, the Lakeside Scenic Zone and the Scenic Forest Zone also have significant contributions, maintaining levels above 16.7% (biomass), 15.8% (NPP), 16.2% (biomass), and 15.9% (NPP) respectively. Notably, in 2020, the biomass values of both the Lakeside Scenic Zone and the Scenic Forest Zone surpassed those of the Exotic Garden Zone, reaching 849.35 tons of carbon and 828.92 tons of carbon, respectively. Since the park's free admission policy began in 2021, the Native Countryside Zone has shown the most significant increase in CS capacity, with growth rates of 31.03% (biomass) and 20.53% (NPP).

From the perspective of average CS capacity per unit area, the Scenic Forest Zone has consistently maintained the highest levels of biomass per unit area and NPP per unit area from 2018 to 2023 (Figures 9 and 10), with biomass per unit area around 40 $tC \cdot ha^{-1}$ and NPP per unit area above 6.6 $tC \cdot ha^{-1}$. In contrast, the Lakeside Scenic Zone has

consistently exhibited the lowest levels, fluctuating around 24.0 tC·ha^{-1} (biomass) and 4.0 tC·ha^{-1} (NPP).

3.4.2. Renovation and Construction Work in Century Park

In collaboration with the Century Park renovation design team and park management staff, the details of the renovation projects implemented in each zone of Century Park are summarized in Table 8, and Figure 11 illustrates the spatial distribution of the renovation nodes within the park.

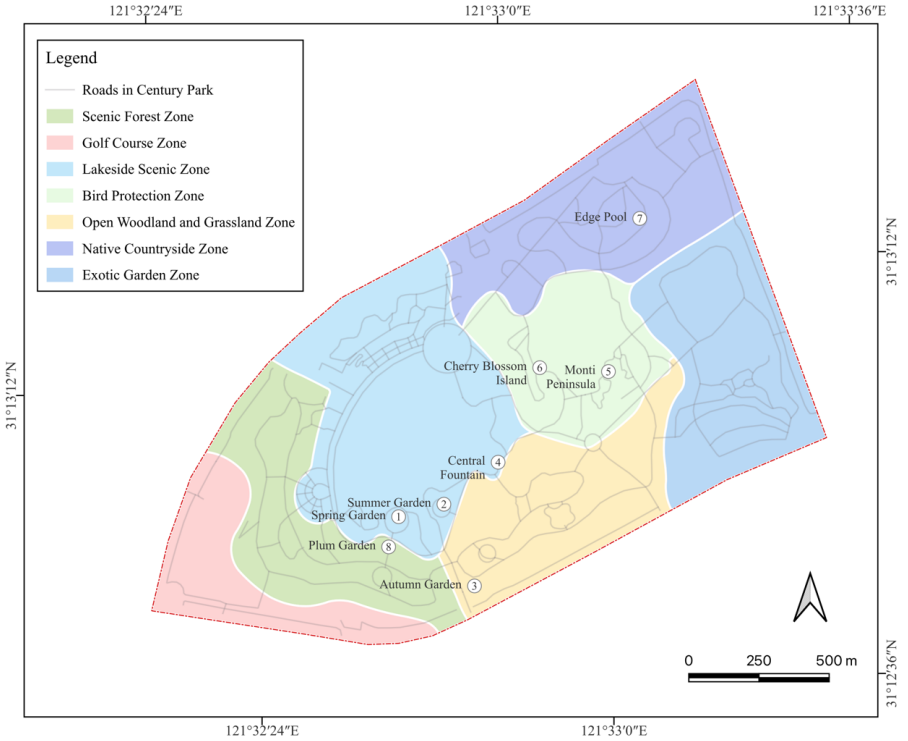


Figure 11. Spatial distribution of renovation and construction work in Century Park.

Table 8. Descriptions of renovation and construction work in Century Park.

Zone	Vegetation Renewal and Improvement Measures	Node	Node-Specific Greenery Improvement Measures
Lakeside Scenic Zone	Replace evergreen shrubs with perennial herbaceous flowering shrubs and grasses to enrich ground cover color.	Spring Garden	Adjust plant configuration, increasing the proportion of flowering plants.
		Summer Garden	Thin out dense plants and organize the disordered vegetation.
Open Woodland and Grassland Zone	Enrich understory planting layers with additional flowering shrubs and grasses, and plant flower paths along forest edges.	Autumn Garden	Plant Osmanthus trees along the site edges and add Starwort and other herbs at the boundaries.
		Central Fountain	Install ecological floating islands and plant aquatic plants.
Bird Protection Zone		Monti Peninsula	Transform the central area of Monti Peninsula into horticultural facilities with arranged garden displays.
		Cherry Blossom Island	Enrich cherry varieties on Cherry Blossom Island according to the park's climate and surroundings; plant cherry trees along the pathway from Entrance 2 to Cherry Blossom Island for botanical guidance.

Table 8. *Cont.*

Zone	Vegetation Renewal and Improvement Measures	Node	Node-Specific Greenery Improvement Measures
Native Countryside Zone		Edge Pool	Increase the planting of grasses to emphasize seasonal countryside landscapes; add rice, reeds, and other plants around the edge of the pool, covering an area of 1.1 hectares.
Scenic Forest Zone	Perform selective thinning in the northern section; add autumn foliage trees and plant colored-leaf trees in the western section.	Plum Garden	Organize plantings and increase the number of medium-sized trees to enhance plant diversity.
Golf Course Zone	Renovate the northern management office area and surrounding sites, removing some trees and shrubs.		

3.4.3. Subsubsection

To determine the changes in the five biotope types within each zone and further explore the reasons for changes in CS capacity, we selected three specific areas as examples: the Lakeside Scenic Zone, the Scenic Forest Zone, and the Golf Course Zone.

1. Lakeside Scenic Zone

In the Lakeside Scenic Zone, the area of evergreen trees increased from 5.48 ha in 2018 to 7.05 ha in 2023, with a total increase of approximately 1.57 ha, representing a growth rate of about 28.63% (Figure 12). Conversely, the area of deciduous trees slightly decreased from 7.30 ha in 2018 to 6.03 ha in 2023, with a total decrease of approximately 1.27 ha, representing a reduction of about 17.40%. The areas of water bodies and grasslands remained relatively stable, with minor fluctuations. The area of sealed surfaces increased from 2.05 ha in 2018 to 2.94 ha in 2023, with a total increase of approximately 0.89 ha, representing a growth rate of about 43.41%.

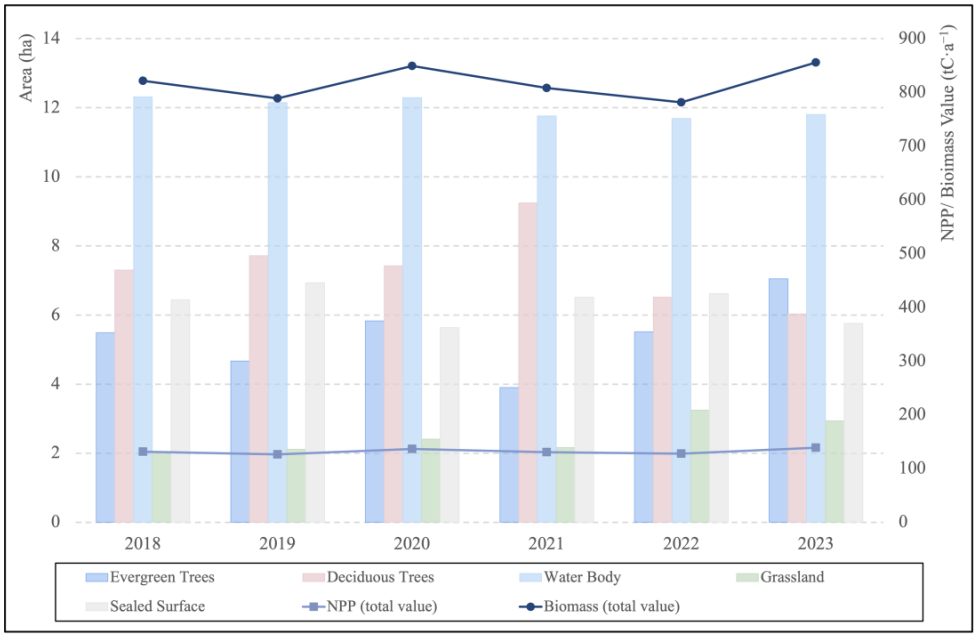


Figure 12. Variation in area of 5 biotopes and CS capacity in Lakeside Scenic Zone.

2. Scenic Forest Zone

In the Scenic Forest Zone, the area of evergreen trees remained relatively stable between 2018 and 2021, fluctuating between 6.6 and 7.1 ha (Figure 13). From 2021 onwards, the area of evergreen trees increased significantly from 6.08 ha to 7.64 ha, representing a

growth rate of 25.66%. The area of deciduous trees showed an opposite trend, decreasing from 8.35 ha in 2018 to 7.60 ha in 2021, reaching a peak of 8.43 ha in 2022, and then decreasing again by 2.54 ha over two years, with annual reductions of 21.11% and 11.43%. The areas of water bodies and sealed surfaces remained relatively stable, fluctuating around 2.0 ha and 1.7 ha, respectively. The area of lawns showed a gradual upward trend, with a total increase of 1.75 ha and an annual growth rate of 46.51%.

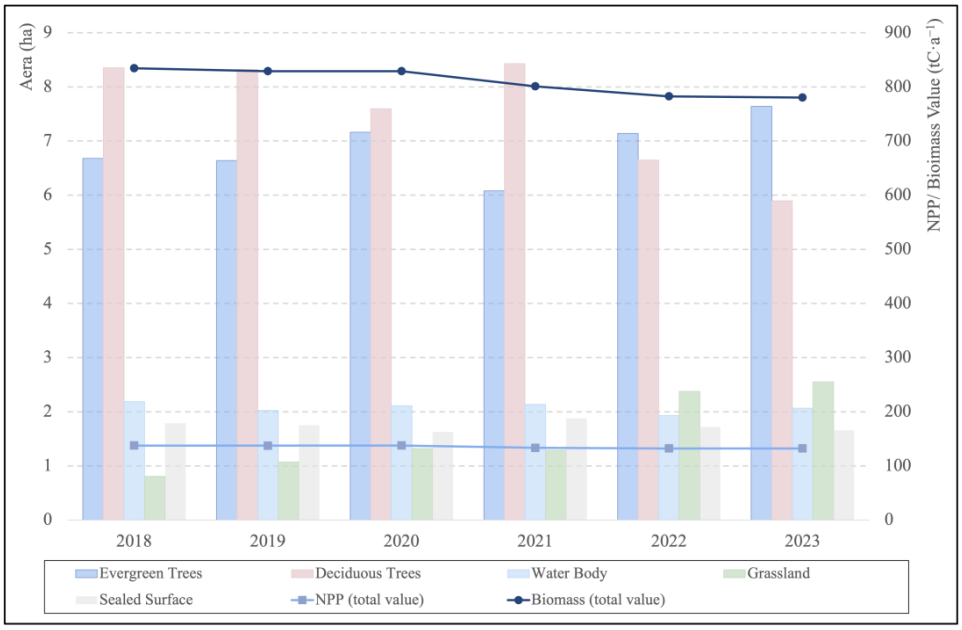


Figure 13. Variation in area of 5 biotopes and CS capacity in Scenic Forest Zone.

3. Golf Course Zone

In the Golf Course Zone, the areas of evergreen and deciduous trees experienced minimal changes, with minor fluctuations (Figure 14). The areas of water bodies and grasslands remained relatively stable, with minor changes. The area of sealed surfaces increased from 1.64 ha in 2018 to 2.16 ha in 2023, with a total increase of approximately 0.52 ha, representing a growth rate of about 31.71%.

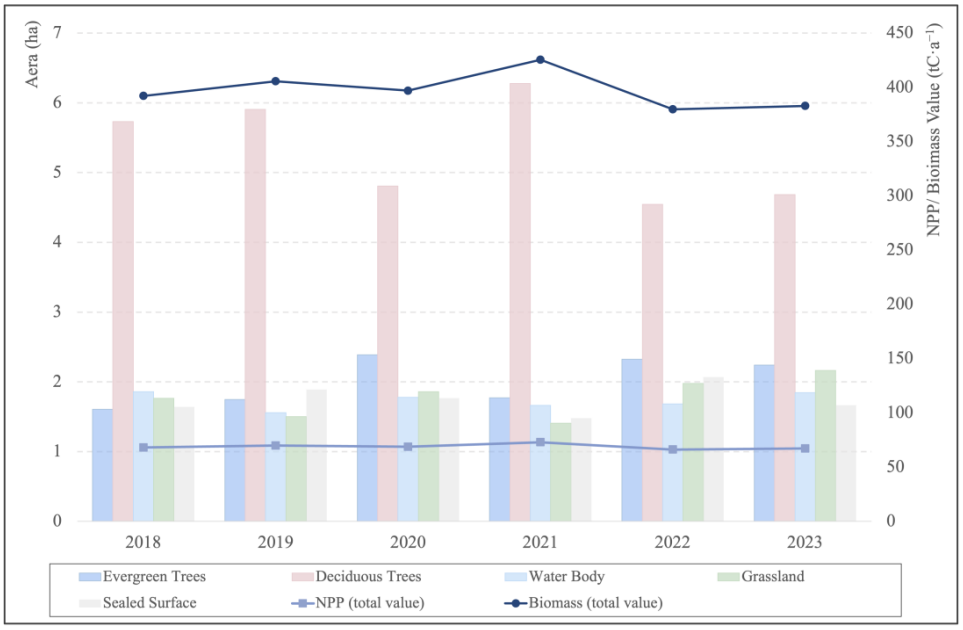


Figure 14. Variation in area of 5 biotopes and CS capacity in Golf Course Zone.

4. Discussion

4.1. CS Capacity in Urban Parks and Influencing Factors

4.1.1. Comparison of CS Capacity in Urban Parks

The CS capacity of Century Park, as indicated by its NPP of 5.73–5.88 $tC \cdot hm^{-2} \cdot a^{-1}$ and biomass of 32.88–34.12 $tC \cdot hm^{-2}$, is significantly higher than the average for vegetation in Shanghai's built-up areas; the NPP is 1.45 $tC \cdot hm^{-2} \cdot a^{-1}$ and the biomass is 17.01 $tC \cdot hm^{-2}$ (Table 9).

Table 9. Comparison of NPP and biomass in urban parks.

Study Area	NPP ($tC \cdot hm^{-2} \cdot a^{-1}$)	Biomass ($tC \cdot hm^{-2}$)	Source
Forests in China	6.5	36–38.9	[51,52]
Urban forests in Shanghai	0.625	47.8	[53]
Vegetation inside Shanghai built-up area	1.45	17.01	[54,55]
Park green spaces in Shanghai	5.00 (inside built-up area)/ 6.86 (outside built-up area)	/	[20]
10 urban parks in India	/	32.85 (on average)	[14]
Shanghai Century Park	5.73–5.88	32.88–34.12	this study

In contrast to Shanghai's urban forests, whose NPP value is 0.625 $tC \cdot hm^{-2} \cdot a^{-1}$, Century Park exhibits a significantly higher NPP, exceeding 5.7 $tC \cdot hm^{-2} \cdot a^{-1}$.

Additionally, Century Park's NPP exceeds the average NPP for park green spaces within Shanghai's built-up areas, which stands at 5.00 $tC \cdot hm^{-2} \cdot a^{-1}$, suggesting that the vegetation in Century Park is in relatively good condition and that the park's carbon sequestration capacity is at a high level. However, the results of Xu's study demonstrated that parks located outside the built-up area possess higher NPP values in comparison with those within the built-up area, which are also greater than the NPP value of Century Park. This phenomenon can be explained by the fact that human activities exert a considerable influence over the park's CS capacity.

When compared to natural forests in China, where the average NPP is approximately 6.5 $tC \cdot hm^{-2} \cdot a^{-1}$ and biomass ranges from 36 to 38.9 $tC \cdot hm^{-2}$, Century Park, as an artificial green space, shows a slightly lower CS capacity. The variation may be attributed to the relatively shorter growth period of Century Park, leading to less accumulated biomass. However, the park's NPP value, which indicates a high photosynthetic rate or productivity, i.e., high carbon sequestration efficiency, is comparable to that of natural forests. As a matter of fact, this finding demonstrates the substantial CS potential of Century Park, contributing effectively to urban carbon sequestration and CO_2 emission reduction efforts.

4.1.2. Factors Influencing CS Capacity of Century Park

In general, the CS capacity of Century Park exhibited notable fluctuations between 2018 and 2023. The decline in biomass and NPP from 2018 to 2020 can be attributed to vegetation adjustments within the park, including the removal of aging plants and the thinning of densely planted areas. These activities reduced biomass and NPP by 2.20% and 0.86%, respectively. In contrast, the subsequent increase in biomass (1.05%) and NPP (0.51%) from 2020 to 2021 likely resulted from the completion of renovation projects, which stabilized vegetation growth and enhanced CS capacity. The decrease in biomass (1.45%) and NPP (0.64%) from 2021 to 2022 may be linked to increased visitor activity following the introduction of free admission. Visitor impacts, such as trampling and vegetation damage, likely inhibited biomass accumulation during this period. However, from 2022 to 2023, improvements in park maintenance and management, alongside the completion of vegetation restoration, led to a significant recovery in terms of biomass (3.78%) and NPP (2.74%), reflecting a notable enhancement in carbon sequestration capacity.

Overall, the observed fluctuations in the CS capacity of Century Park underscore the sensitivity of the park's vegetation to human interventions, including construction

and renovation activities and visitor behaviors. With effective management and minimal disturbances, Century Park has the potential for continued growth in carbon storage and sequestration.

The variations in CS capacity across the three zones directly reflect the impacts of renovation activities and management practices. In the Lakeside Scenic Zone, the increase in evergreen forest area and the corresponding decrease in deciduous forest, alongside changes in water bodies, lawns, and sealed surfaces, reflect the impact of recent renovation efforts. The thinning and transplantation of vegetation in specific nodes have altered the spatial distribution of different biotope types, which in turn has affected the CS capacity of this zone. The overall decline in CS capacity observed during this period can be attributed to these changes in vegetation structure and biotope types.

The Scenic Forest Zone underwent significant updates, including the reconfiguration of planting spaces and thinning of dense forests. These changes were aimed at enhancing the scenic features of the zone, but led to a reduction in CS capacity in the short term. The updates have influenced the stability and growth of different vegetation types, indicating that, while renovations can enhance aesthetic and functional aspects of the park, they can also impact ecosystem services, including CS.

In the Golf Course Zone, renovations involving vegetation removal and an increase in sealed surfaces have led to a reduction in CS capacity. The changes in biotope types, particularly the increase in sealed surfaces, highlight the trade-offs between park functionality and ecosystem services. This period underscores the need to balance construction and renovation activities with the preservation of ecosystem functions to maintain the overall CS capacity of urban parks.

4.2. Implications for Park Construction and Management

4.2.1. Optimizing Tree Species Selection and Arrangement

From an absolute value perspective, the CS capacity per unit area of evergreen trees is higher than that of deciduous trees. Both forest types contribute positively to the CS of urban parks. Therefore, when updating and renovating park vegetation with the goal of high CS, the trade-offs between evergreen and deciduous trees' CS capacity can be minimized. Adjustments to the proportions of evergreen and deciduous trees should be made according to specific landscape needs. This could help not to only achieve optimal CS efficiency, but also to enhance ecosystem stability and sustainability.

For example, in private spaces or areas providing recreational functions, sparse-branching, low-canopy evergreen species can be selected. In contrast, tall deciduous species are suitable for plazas requiring sunlight during winter, ensuring sun exposure in winter and shade in summer. For ornamental green walls or gardens that require year-round aesthetic appeal, a mix of evergreen and deciduous species can be considered to maintain landscape diversity and persistence. In the Shanghai region, tree species with strong CS capabilities include *Cinnamomum camphora* (L.) J. Presl, *Pistacia chinensis* Bunge, *Ulmus parvifolia* Jacq., *Bischofia polycarpa* (Lévl.) Airy Shaw, and *Zelkova serrata* (Thunb.) Makino [56,57]. Therefore, for urban parks in Shanghai, these tree species should be prioritized in planting designs and arrangements.

4.2.2. Scientifically Adjusting Planting Density

Thinning and transplanting tree communities in Century Park negatively impacted the park's short-term CS capacity. However, from the perspective of long-term vegetation growth, adjusting planting density should benefit vegetation growth and enhance the park's CS efficiency. To boost the overall CS capacity of park vegetation, a near-natural, multi-layered, mixed-age structure should be considered for creating high-density, high-CS plant communities. This will increase community complexity, fostering stable, symbiotic relationships among various plant types and thereby improving overall CS efficiency. This configuration also enriches landscape layers and effectively segregates spaces, being suitable for plant landscape nodes, private areas, or protective boundaries.

For low-density, high-CS plant communities, tall trees with low density can be arranged to create open under-canopy spaces, enhancing openness. These can be used along roadsides, in sparse woodland lawns, or in open plazas.

4.2.3. Improving CS Capacity in Low-CS Areas

For grassland with relatively low CS capacity, interplanting trees within or along the boundaries where feasible for aesthetic and landscape needs could effectively increase the overall CS potential of these areas.

Similarly, water bodies with limited CS capacity could benefit from integrating low-carbon aquatic plants into their surrounding landscape. Species such as *Nymphaea tetragona* L. and *Acorus calamus* L. have strong carbon absorption and fixation capacities [58]. Thus, incorporating these plants in parks can significantly enhance organic carbon storage within water bodies.

In addition, low-carbon renovation could improve the CS potential of sealed surfaces. For instance, converting hard-paved areas to permeable, breathable materials supplemented with vegetation can increase carbon absorption. Vertical greening and rooftop gardens on park buildings provide further options to expand green coverage, thereby contributing to the overall CS capacity of urban parks.

4.2.4. Enhancing Park Management Capacity

When analyzing the factors influencing CS capacity changes in Century Park, human factors showed a significant impact on the park's CS capacity. Effective park management ensures healthy plant growth, reducing plant mortality and replacement and thereby achieving increased CS and emission reduction. Therefore, in the daily operation and maintenance of urban parks, increasing the professionalism of management departments; enhancing plant protection and maintenance; and implementing effective measures to prevent damage from pests, natural disasters, and other threats is essential. Additionally, regulating visitor activities during daily park visits to reduce damage caused by uncivilized behavior ensures a stable growth environment for plants. These management and governance strategies can further enhance the long-term CS capacity of urban parks.

4.3. Limitations and Future Research Prospects

The limitations of this study are primarily as follows:

Firstly, we classified urban park biotopes through visual interpretation and the RF model. However, due to the precision limitations of Sentinel-2 imagery used in this study, the classification results may be subject to some degree of bias. Utilizing technologies such as LiDAR to acquire data on land cover types and planting structures within parks can improve the accuracy of raw data. This approach would allow for more detailed and accurate mapping of mixed areas with complex habitat elements and structures, thus enabling a more refined and comprehensive CS capacity assessment. Additionally, urban parks rely on both vegetation and soil for CS, but this study did not consider soil CS capacity and focused only on the changes in above-ground biotope CS capacity in two dimensions. Future research should explore effective methods for measuring soil CS capacity and analyze the impact of vertical structure characteristics on CS capacity.

Secondly, this study analyzed the reasons for the spatiotemporal variations in park CS capacity from a management practice perspective. In reality, the CS capacity of urban parks is influenced by many factors, such as environmental changes, regional microclimate variability, and biodiversity. To accurately predict the sustainability of parks under different environmental pressures, it is crucial to analyze the impact characteristics of multiple factors on park CS.

Additionally, as complex ecosystems, urban parks provide diverse ecosystem services. To maximize the ecological functions of urban parks, it is necessary to find a balance between CS functions and other ecosystem services and explore potential threshold effects to achieve the synergy and optimization of ecosystem services.

5. Conclusions

In this study, we conducted an in-depth spatial–temporal analysis of the CS capacity of Century Park, aiming to provide a scientific basis for the CS management and planning of urban parks. Using biotope mapping, we integrated remote sensing data with a Random Forest model for precise CS estimation and explored the impact of park management on its spatiotemporal variations. The main findings are as follows:

1. The classification results from the RF model indicated that winter imagery data provided higher accuracy and consistency in biotope classification compared to summer imagery. Moreover, incorporating vegetation indices into the classification model proved to significantly improve accuracy, underscoring the importance of multi-source data in enhancing remote sensing classification accuracy.
2. The CS capacity of Century Park exhibited a fluctuating upward trend from 2018 to 2023. Through annual biotope mapping, significant differences in CS capacity were observed among different biotopes within the park. Exotic garden areas contributed over 17% to both biomass and NPP, while the CS capacity of water bodies and sealed surfaces remained relatively stable.
3. This study revealed a correlation between changes in biotope area and CS capacity within Century Park. Between 2018 and 2020, the areas of grasslands and deciduous trees increased, while between 2020 and 2023, evergreen tree areas significantly expanded, primarily due to the conversion from deciduous forests. Vegetation renewal projects in the Lakeside Scenic Zone and Scenic Forest Zone positively impacted CS capacity. However, in the Golf Course Zone, CS capacity declined between 2021 and 2022 due to vegetation removal and the increase in sealed surfaces.

In conclusion, urban parks play a crucial role in urban carbon cycling, serving as significant carbon sinks that help maintain the carbon balance within cities. This study provides a comprehensive spatial–temporal assessment of the CS capacity of Century Park and offers applicable methods and strategies for the CS management of other urban parks. This is of great importance for reducing urban carbon emissions and mitigating the impacts of climate change.

Author Contributions: Conceptualization, N.D. and Y.W.; methodology, Y.W. and J.Y.; software, Y.W.; validation, Y.W.; formal analysis, Y.W.; investigation, W.W. and Y.W.; resources, N.D.; data curation, Y.W. and W.W.; writing—original draft preparation, Y.W. and J.Y.; writing—review and editing, Y.W., J.Y., W.W. and N.D.; visualization, Y.W.; supervision, N.D.; funding acquisition, N.D. All authors have read and agreed to the published version of the manuscript.

Funding: This research was funded by the Special Funds of the Tongji University for "Sino-German Cooperation 2.0 Strategy, grant number ZD2023007; The Key Laboratory of Ecology and Energy Saving Study of Dense Habitat (Tongji University), Ministry of Education, in collaboration with Shanghai Tongji Urban Planning and Design Institute Co., Joint Open Topic of 2022, grant number KY-2022-LH-A05; University-Industry Collaborative Education Program, Ministry of Education, PRC, grant number 231100155154454.

Data Availability Statement: The raw data supporting the conclusions of this article will be made available by the authors upon request.

Acknowledgments: We would first like to express our gratitude to Harald Zepp, Malte Bührs, Lars Gruenhagen, Tian Zhang, and Jiaqi Han for their valuable insights on the methodology in this study. Additionally, we acknowledge Zepp and his team for developing the IMECOGIP toolbox (now known as EnhancES) for assessing the ecosystem services of urban green infrastructures, which significantly supported the quantification of carbon sequestration capacity in this study. Finally, we thank the three anonymous reviewers for their helpful suggestions to improve this study.

Conflicts of Interest: Author Weixuan Wei was employed by the company Future Urban (Shanghai) Design Consulting Co., Ltd. The remaining authors declare that the research was conducted in the absence of any commercial or financial relationships that could be construed as a potential conflict of interest.

Appendix A

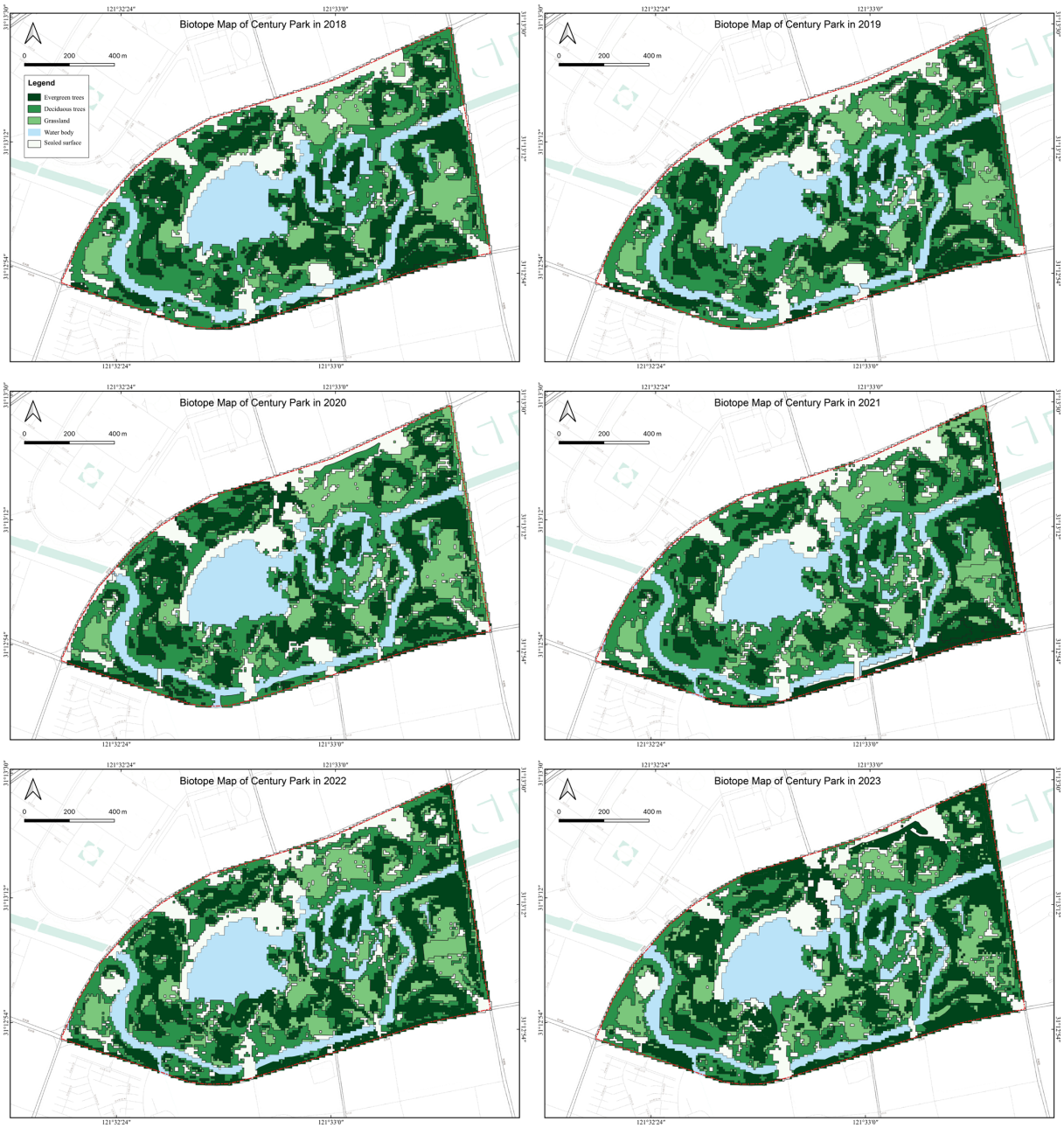


Figure A1. Biotope maps of Century Park from 2018 to 2023.

References

1. *Thriving: Making Cities Green, Resilient, and Inclusive in a Changing Climate*; World Bank: Washington, DC, USA, 2023; ISBN 978-1-4648-1935-3.
2. Mexia, T.; Vieira, J.; Príncipe, A.; Anjos, A.; Silva, P.; Lopes, N.; Freitas, C.; Santos-Reis, M.; Correia, O.; Branquinho, C.; et al. Ecosystem Services: Urban Parks under a Magnifying Glass. *Environ. Res.* **2018**, *160*, 469–478. [CrossRef] [PubMed]
3. Zhang, Y.; Meng, W.; Yun, H.; Xu, W.; Hu, B.; He, M.; Mo, X.; Zhang, L. Is Urban Green Space a Carbon Sink or Source?—A Case Study of China Based on LCA Method. *Environ. Impact Assess. Rev.* **2022**, *94*, 106766. [CrossRef]
4. Zhuang, Q.; Shao, Z.; Li, D.; Huang, X.; Li, Y.; Altan, O.; Wu, S. Impact of Global Urban Expansion on the Terrestrial Vegetation Carbon Sequestration Capacity. *Sci. Total Environ.* **2023**, *879*, 163074. [CrossRef] [PubMed]
5. Shadman, S.; Ahanaf Khalid, P.; Hanafiah, M.M.; Koyande, A.K.; Islam, A.; Bhuiyan, S.A.; Sin Woon, K.; Show, P.-L. The Carbon Sequestration Potential of Urban Public Parks of Densely Populated Cities to Improve Environmental Sustainability. *Sustain. Energy Technol. Assess.* **2022**, *52*, 102064. [CrossRef]

6. Singkran, N. Carbon Sink Capacity of Public Parks and Carbon Sequestration Efficiency Improvements in a Dense Urban Landscape. *Environ. Monit. Assess.* **2022**, *194*, 750. [CrossRef]
7. Zhao, L.; Du, M.; Du, W.; Guo, J.; Liao, Z.; Kang, X.; Liu, Q. Evaluation of the Carbon Sink Capacity of the Proposed Kunlun Mountain National Park. *Int. J. Environ. Res. Public Health* **2022**, *19*, 9887. [CrossRef]
8. Cramer, W.; Kicklighter, D.W.; Bondeau, A.; Iii, B.M.; Churkina, G.; Nemry, B.; Ruimy, A.; Schloss, A.L.; The Participants of The Potsdam NPP Model Intercomparison. Comparing Global Models of Terrestrial Net Primary Productivity (NPP): Overview and Key Results. *Glob. Chang. Biol.* **1999**, *5*, 1–15. [CrossRef]
9. Field, C.B. Sharing the Garden. *Science* **2001**, *294*, 2490–2491. [CrossRef]
10. Bandaru, V.; West, T.O.; Ricciuto, D.M.; César Izaurralde, R. Estimating Crop Net Primary Production Using National Inventory Data and MODIS-Derived Parameters. *ISPRS J. Photogramm. Remote Sens.* **2013**, *80*, 61–71. [CrossRef]
11. Liu, Z.; Hu, M.; Hu, Y.; Wang, G. Estimation of Net Primary Productivity of Forests by Modified CASA Models and Remotely Sensed Data. *Int. J. Remote Sens.* **2018**, *39*, 1092–1116. [CrossRef]
12. Kil, S.H.; Lee, D.K.; Park, G.S.; Lee, S.J.; Ohga, S. Differences in Carbon Sink by Land Use Using Topographic Correction in Seoul, South Korea. *J. Fac. Agric. Kyushu Univ.* **2016**, *61*, 7–15. [CrossRef]
13. Poley, L.G.; McDermid, G.J. A Systematic Review of the Factors Influencing the Estimation of Vegetation Aboveground Biomass Using Unmanned Aerial Systems. *Remote Sens.* **2020**, *12*, 1052. [CrossRef]
14. Dash, S.A.; Pradhan, A.; Behera, N. Estimation of Above-Ground Biomass and Carbon Stock of Tree Species in Public Parks of Bhubaneswar, Odisha. *Arboric. J.* **2022**, *44*, 72–83. [CrossRef]
15. Kim, J.; Kang, Y.; Kim, D.; Son, S.; Kim, E.J. Carbon Storage and Sequestration Analysis by Urban Park Grid Using I-Tree Eco and Drone-Based Modeling. *Forests* **2024**, *15*, 683. [CrossRef]
16. Wang, Y.; Chang, Q.; Li, X. Promoting Sustainable Carbon Sequestration of Plants in Urban Greenspace by Planting Design: A Case Study in Parks of Beijing. *Urban For. Urban Green.* **2021**, *64*, 127291. [CrossRef]
17. Zhao, D.; Cai, J.; Shen, S.; Liu, Q.; Lan, Y. Nature-Based Solutions: Assessing the Carbon Sink Potential and Influencing Factors of Urban Park Plant Communities in the Temperate Monsoon Climate Zone. *Sci. Total Environ.* **2024**, *950*, 175347. [CrossRef]
18. Cimburova, Z.; Barton, D.N. The Potential of Geospatial Analysis and Bayesian Networks to Enable I-Tree Eco Assessment of Existing Tree Inventories. *Urban For. Urban Green.* **2020**, *55*, 126801. [CrossRef]
19. Lu, D. The Potential and Challenge of Remote Sensing-based Biomass Estimation. *Int. J. Remote Sens.* **2006**, *27*, 1297–1328. [CrossRef]
20. Xu, F.; Wang, X.; Li, L. NPP and Vegetation Carbon Sink Capacity Estimation of Urban Green Space Using the Optimized CASA Model: A Case Study of Five Chinese Cities. *Atmosphere* **2023**, *14*, 1161. [CrossRef]
21. Li, X.; Jiang, Y.; Liu, Y.; Sun, Y.; Li, C. The Impact of Landscape Spatial Morphology on Green Carbon Sink in the Urban Riverfront Area. *Cities* **2024**, *148*, 104919. [CrossRef]
22. Chamberlin, A.J.; Liu, Z.Y.-C.; Cross, C.G.L.; Pourtois, J.; Siregar, I.Z.; Nurrochmat, D.R.; Setiawan, Y.; Webb, K.; Hopkins, S.; Sokolow, S.H.; et al. Improving Remote Monitoring of Carbon Stock in Tropical Forests Using Machine Learning: A Case Study in Indonesian Borneo. *Remote Sens.* **2024**, *preprint*. [CrossRef]
23. Park, S.-I.; Um, J.-S. Differentiating Carbon Sinks versus Sources on a University Campus Using Synergistic UAV NIR and Visible Signatures. *Environ. Monit. Assess.* **2018**, *190*, 652. [CrossRef]
24. Huete, A.R. Vegetation Indices, Remote Sensing and Forest Monitoring. *Geogr. Compass* **2012**, *6*, 513–532. [CrossRef]
25. Lu, D.; Mausel, P.; Brondízio, E.; Moran, E. Relationships between Forest Stand Parameters and Landsat TM Spectral Responses in the Brazilian Amazon Basin. *For. Ecol. Manag.* **2004**, *198*, 149–167. [CrossRef]
26. Lv, Y.; Han, N.; Du, H. Estimation of Bamboo Forest Aboveground Carbon Using the RGLM Model Based on Object-Based Multiscale Segmentation of SPOT-6 Imagery. *Remote Sens.* **2023**, *15*, 2566. [CrossRef]
27. Şahin Körmeçli, P.; Seçkin Gündoğan, G. Assessment of Vegetation Change Using NDVI, LST, and Carbon Analyses in Çankırı Karatekin University, Turkey. *Environ. Monit Assess* **2024**, *196*, 331. [CrossRef]
28. Tamondong, A.; Cruz, C.; Quides, R.R.; Garcia, M.; Cruz, J.A.; Guihawan, J.; Blanco, A. Remote Sensing-Based Estimation of Seagrass Percent Cover and LAI for above Ground Carbon Sequestration Mapping. In *Remote Sensing of the Open and Coastal Ocean and Inland Waters*; SPIE: Bellingham, WA, USA, 2018; Volume 10778, p. 1077803.
29. Mngadi, M.; Odindi, J.; Mutanga, O. Quantifying Carbon Stock Variability of Species Within a Reforested Urban Landscape Using Texture Measures Derived from Remotely Sensed Imagery. In *Advances in Remote Sensing for Forest Monitoring*; John Wiley & Sons, Ltd.: Hoboken, NJ, USA, 2022; pp. 150–166, ISBN 978-1-119-78815-7.
30. Forman, R.T.T. *Land Mosaics: The Ecology of Landscapes and Regions*; Cambridge University Press: Cambridge, UK, 1995; ISBN 978-0-521-47980-6.
31. Sukopp, H.; Weiler, S. Biotope Mapping and Nature Conservation Strategies in Urban Areas of the Federal Republic of Germany. *Landsc. Urban Plan.* **1988**, *15*, 39–58. [CrossRef]
32. Michael, B. Remote Sensing and GIS-Based Techniques for the Classification and Monitoring of Biotopes: Case Examples for a Wet Grass-and Moor Land Area in Northern Germany. *J. Nat. Conserv.* **2003**, *11*, 145–155. [CrossRef]
33. Qiu, L.; Gao, T.; Gunnarsson, A.; Hammer, M.; von Bothmer, R. A Methodological Study of Biotope Mapping in Nature Conservation. *Urban For. Urban Green.* **2010**, *9*, 161–166. [CrossRef]

34. Zhao, C.; Yang, Y.-Q.; Hu, Y.-D. Methodology, Assessment and Application of Biotope Mapping for Urban Parks in China: A Case Study on Riverside Park, Yichang. *Front. Environ. Sci.* **2022**, *10*, 1008362. [CrossRef]
35. Lee, K.-J.; Han, B.-H.; Lee, S.-D. Ecological Management Plan and Biotope Structure of Namsan Urban Natural Park in Seoul. *J. Korean Inst. Landsc. Archit.* **2004**, *32*, 102–118.
36. Gratani, L.; Varone, L.; Bonito, A. Carbon Sequestration of Four Urban Parks in Rome. *Urban For. Urban Green.* **2016**, *19*, 184–193. [CrossRef]
37. Jo, H.-K.; Kim, J.-Y.; Park, H.-M. Carbon Reduction and Planning Strategies for Urban Parks in Seoul. *Urban For. Urban Green.* **2019**, *41*, 48–54. [CrossRef]
38. *The General Office of the Shanghai Municipal People's Government Shanghai's 13th Five-Year Plan for Energy Conservation, Emission Reduction, and Comprehensive Greenhouse Gas Control Work Program*; The General Office of the Shanghai Municipal People's Government: Shanghai, China, 2018.
39. Zhang, Z.; Ren, Y.; Dong, H. Research on Carbon Emissions Peaking and Low-Carbon Development of Cities: A Case of Shanghai. *Environ. Eng.* **2020**, *38*, 12–18. [CrossRef]
40. *Shanghai Municipal Development & Reform Commission Key Work Arrangements for Carbon Peak, Carbon Neutrality, and Energy Conservation and Emission Reduction in Shanghai for 2024*; Shanghai Municipal Development & Reform Commission: Shanghai, China, 2024.
41. Jia, X.; Han, H.; Feng, Y.; Song, P.; He, R.; Liu, Y.; Wang, P.; Zhang, K.; Du, C.; Ge, S.; et al. Scale-Dependent and Driving Relationships between Spatial Features and Carbon Storage and Sequestration in an Urban Park of Zhengzhou, China. *Sci. Total Environ.* **2023**, *894*, 164916. [CrossRef] [PubMed]
42. Ma, L.; Li, M.; Ma, X.; Cheng, L.; Du, P.; Liu, Y. A Review of Supervised Object-Based Land-Cover Image Classification. *ISPRS J. Photogramm. Remote Sens.* **2017**, *130*, 277–293. [CrossRef]
43. Spadoni, G.L.; Cavalli, A.; Congedo, L.; Munafò, M. Analysis of Normalized Difference Vegetation Index (NDVI) Multi-Temporal Series for the Production of Forest Cartography. *Remote Sens. Appl. Soc. Environ.* **2020**, *20*, 100419. [CrossRef]
44. Wang, Q.; Tenhunen, J.D. Vegetation Mapping with Multitemporal NDVI in North Eastern China Transect (NECT). *Int. J. Appl. Earth Obs. Geoinf.* **2004**, *6*, 17–31. [CrossRef]
45. Song, L.; Li, M.; Xu, H.; Guo, Y.; Wang, Z.; Li, Y.; Wu, X.; Feng, L.; Chen, J.; Lu, X.; et al. Spatiotemporal Variation and Driving Factors of Vegetation Net Primary Productivity in a Typical Karst Area in China from 2000 to 2010. *Ecol. Indic.* **2021**, *132*, 108280. [CrossRef]
46. Wei, X.; Yang, J.; Luo, P.; Lin, L.; Lin, K.; Guan, J. Assessment of the Variation and Influencing Factors of Vegetation NPP and Carbon Sink Capacity under Different Natural Conditions. *Ecol. Indic.* **2022**, *138*, 108834. [CrossRef]
47. Bührs, M.; Busch, C.; Falke, M.; Gruenhagen, L.; Inostroza, L.; Zepp, H.; EnhancES. The IMECOGIP Toolbox: Handbook; Ruhr University Bochum, Geographical Institute. 2024. Available online: https://www.geographie.ruhr-uni-bochum.de/physik/imecogip.html.de (accessed on 15 October 2024).
48. Cannell, M.G.R. *World Forest Biomass and Primary Production Data*; Academic Press Inc.: Cambridge, MA, USA, 1982; ISBN 978-0-12-158780-2.
49. Mitchell, C.P.; Zsuffa, L.; Andersson, S.; Stevens, D.J. *Forestry, Forest Biomass, and Biomass Conversion: The IEA Bioenergy Agreement (1986–1989) Summary Reports*; Elsevier Applied Science: Amsterdam, The Netherlands, 1990; ISBN 978-1-85166-443-6.
50. Wang, Z. The Analysis of Practice on Enhancing the Ecologically Scenic Function in Shanghai Century Park. Master's Thesis, Shanghai Jiao Tong University, Shanghai, China, 2009.
51. Yang, J.; Ji, X.; Deane, D.C.; Wu, L.; Chen, S. Spatiotemporal Distribution and Driving Factors of Forest Biomass Carbon Storage in China: 1977–2013. *Forests* **2017**, *8*, 263. [CrossRef]
52. Zhu, W.; Pan, Y.; Long, Z.; Chen, Y.; Li, J.; Hu, H. Estimating Net Primary Productivity of Terrestrial Vegetation Based on GIS and RS: A Case Study in Inner Mongolia, China. *Natl. Remote Sens. Bull.* **2005**, *9*, 300–307.
53. Xu, F.; Liu, W.; Ren, W.; Zhong, Q.; Zhang, G.; Wang, K. Effects of Community Structure on Carbon Fixation of Urban Forests in Shanghai, China. *Chin. J. Ecol.* **2010**, *29*, 439–447. [CrossRef]
54. Chen, W.Y. The Role of Urban Green Infrastructure in Offsetting Carbon Emissions in 35 Major Chinese Cities: A Nationwide Estimate. *Cities* **2015**, *44*, 112–120. [CrossRef]
55. Shi, Y. Veretation Structure Characteristics and Carbon Uptake of Urban Built-up Area in China. Ph.D. Thesis, Zhejiang University, Hangzhou, China, 2013.
56. Chen, Y. 20-Year Dynamics Changes of Plant Communities in Shanghai Typical Urban Green Space. Master's Thesis, Central South University of Forestry and Technology, Changsha, China, 2021.
57. Luo, Y.; Zhang, D.; Zhang, L.; Chen, X. Study on Selection and Collocation of Urban Greening Tree Species under Dual Carbon Goal—A Case Study of Shanghai Expo Park. *Landsc. Archit. Acad. J.* **2022**, *39*, 25–32.
58. Wang, X.; Long, Y.; Yu, L.; Wu, S.; Chen, Q.; Liu, Z.; Zhang, H.; Wang, Y. Effects of aquatic plants on the spatio-temporal variations of CO_2 and CH4 fluxes in urban landscape waters. *Acta Ecol. Sin.* **2023**, *43*, 3592–3606. [CrossRef]

Disclaimer/Publisher's Note: The statements, opinions and data contained in all publications are solely those of the individual author(s) and contributor(s) and not of MDPI and/or the editor(s). MDPI and/or the editor(s) disclaim responsibility for any injury to people or property resulting from any ideas, methods, instructions or products referred to in the content.